Optimal Design of Energy and Spectral Efficiency Tradeoff in One-Bit Massive MIMO Systems

Yongzhi Li, Cheng Tao, *Member, IEEE,* Amine Mezghani, A. Lee Swindlehurst, *Fellow, IEEE*
Gonzalo Seco-Granados, *Senior Member, IEEE,* and Liu Liu, *Member, IEEE,*

arXiv:1612.03271v1 [cs.IT] 10 Dec 2016

***Abstract*—This paper considers a single-cell massive multiple-input multiple-output (MIMO) system equipped with a base station (BS) that uses one-bit quantization and investigates the energy efficiency (EE) and spectral efficiency (SE) trade-off by simultaneously looking at the uplink and downlink transmission. To this end, we first propose a new precoding scheme and downlink power allocation strategy, which makes the uplink-downlink SINR duality hold in the one-bit MIMO systems. Then, by taking into account the effect of the imperfect channel state information (CSI), we obtain approximate closed-form expressions for the uplink achievable rate with maximum ratio combining (MRC) and zero-forcing (ZF) receivers, which, according to the duality property, can also be achieved in the downlink transmission. By employing the multiple objective optimization (MOO) framework, we focus on the optimal design for the EE and SE trade-off that jointly selects the number of active terminals, pilot training duration and operating power to maximize both EE and SE. The weighted Chebyshev method is used to obtain the Pareto boundary of EE and SE, which allows the system to know all the possible operating points and balance the EE and SE in an efficient way. In order to go beyond the Pareto boundary and actually solve the MOO problem, this problem is transformed into a single-objective problem using the a priori method such as the weighted product method, where the operating EE and SE are chosen with equal importance by adjusting the weights. Numerical results are presented to verify our analytical results and demonstrate the fundamental tradeoff between EE and SE for different parameter settings.**

***Index Terms*—massive MIMO, one-bit quantization, resource allocation, spectral efficiency, energy efficiency.**

Y. Li, C. Tao, and L. Liu are with the Institute of Broadband Wireless Mobile Communications, School of Electronic and Information Engineering, Beijing Jiaotong University, Beijing, 100044, China (email: liyongzhi@bjtu.edu.cn; chtao@bjtu.edu.cn; liuliu@bjtu.edu.cn).

G. Seco-Granados is with the Telecommunications and Systems Engineering Department, Universitat Autònoma de Barcelona, Barcelona 08193, Spain (e-mail: gonzalo.seco@uab.es).

A. Mezghani and A. L. Swindlehurst are with the Center for Pervasive Communications and Computing, University of California, Irvine, CA 92697 USA (e-mail: amezghan@uci.edu; swindle@uci.edu). A. L. Swindlehurst is also a Hans Fischer Senior Fellow of the Institute for Advanced Study at the Technical University of Munich.

The research was supported in part by the National 863 Project Granted No. 2014AA01A706, Beijing Natural Science Foundation project Grant No. 2016023, Fundamental Research Funds for the Central Universities under grant 2015JBM011, the NSFC project under grant No. 61471027, the Research Fund of National Mobile Communications Research Laboratory, Southeast University No. 2014D05, and Beijing Natural Science Foundation project under grant No.4152043. A. Swindlehurst was supported by the National Science Foundation under Grant ECCS-1547155, and by the Technische Universität München Institute for Advanced Study, funded by the German Excellence Initiative and the European Union Seventh Framework Programme under grant agreement No. 291763, and by the European Union under the Marie Curie COFUND Program.

I. Introduction

In the past decade, there has been tremendous work to improve system spectral efficiency (SE) and throughput triggered by the spectrum scarcity and the demand for higher rate of the multimedia applications in wireless communication. The massive multiple-input multiple-output (MIMO) technology, known as a worthy candidate technique of the fifth generation (5G) wireless communication systems, has been identified as the key to increase the SE by orders of magnitude over contemporary systems. The main idea of massive MIMO is based on equipping the base stations (BSs) with many antenna elements, which provides unprecedented spatial degrees of freedom for simultaneously serving multiple user terminals on the same time-frequency channel [1]–[4].

However, with a large number of antenna elements deployed at the BS, system cost and power consumption will be excessive if each antenna element and the corresponding radio frequency (RF) chain is equipped with a high-resolution and power-hungry analog-to-digital converter/digital-to-analog converters (ADC/DACs). In addition, as huge bandwidths and correspondingly high sampling rates will be required in next generation wireless systems, high-speed ADCs are either unavailable or too costly for practical implementation [5]. Therefore, the use of low-resolution, especially the one-bit ADC/DACs has been suggested in massive MIMO systems [6]–[9]. The benefits of using one-bit ADC/DACs are two folds: i) They are the least power consuming devices to convert analog/digital signals into digital/analog, and hence, can significantly reduce the power consumption and system cost of the massive MIMO base station; ii) They may only consist of a simple comparator and do not require automatic gain control and highly linear amplifiers, and hence, simplify the analog front end. It has been shown that MIMO capacity is not severely reduced by the coarse quantization at low signal-to-noise ratios (SNRs) [10], and the power penalty due to one-bit quantization is approximately equal to only $\pi/2$ (1.96dB) in the low SNR region [11]. In addition, [8] showed that, compared with the conventional MIMO systems with perfect hardware implementation, the performance loss in one-bit MIMO systems can be compensated with deploying around 2.5 times more antennas at the BS. Therefore the use of one-bit ADC/DACs can make the massive MIMO technique more viable in practice.

Up to now, the SE has been the main performance indicator for designing and optimizing wireless communication networks [12], [13]. Recently, due to the pressure stemming

from environmental concerns and the rapidly increasing cost of energy, the green radio or green communications has attracted considerable research interest [14], [15]. The ultimate goal of the green radio is to improve the energy efficiency (EE) for wireless communication, and hence, to reduce carbon emissions. There has been a large amount of work devoting to maximizing the EE for massive MIMO in various scenarios, including single cell and multi-cell deployment [16], [17]. However, energy efficiency and spectral efficiency are often conflicting objectives, such that improvements in one objective lead to deterioration of another objective. This is because the same available network resources such as the transmit power and the number of terminals, have oppositive effect in each type of efficiency. For example, as shown in [16, Fig. 6], when the system achieves the maximal EE, its corresponding SE is only 9 bits/s/Hz, which is far from being expected in future wireless communication. Therefore, in order to achieve the requirement of high spectral and energy efficiency in next generation wireless communication, recently the attention has shifted to the joint optimization of the EE and SE rather than focusing on either one of the two objectives separately. This leads to a the multiple objective optimization problem, which supports the search for the best attainable operating point [18]–[20].

There has been limited prior work on the EE-SE tradeoff in various wireless communication systems [21]–[24]. Authors in [21] proposed a new paradigm for EE-SE tradeoff for OFDMA cellular network and showed that significant amount of bandwidth can be saved with a slight increase in energy consumption by using the proposed paradigm. In [22], the relationship between EE and SE for the downlink multiuser distributed antennas systems (DAS) is investigated, and an algorithm to allocate the available power to balance EE and SE is also proposed. [23] considered a full-duplex relay system and proposed four typical power-scaling schemes to improve EE. It is also showed in [23] that the proposed schemes achieve good performance tradeoffs between SE and EE. Authors in [24] investigated the SE-EE tradeoff issue by formulating the multi-objective optimization problem subject to maximum total transmission power constrain for downlink massive MIMO system. The fundamental tradeoff between EE and SE for different parameter settings is also demonstrated in [24].

In this paper, we consider a single-cell massive MIMO with a BS equipped with one-bit quantization devices and address the EE-SE tradeoff issue by looking simultaneously at the uplink and downlink transmission. Our goal is to provide insight on how number of active terminals, pilot training length and the system operating power affect the EE and SE for different linear processing schemes in one-bit massive MIMO system. Our specific contributions are summarized below.

- We first provide the signal model for the uplink and downlink transmission in one-bit MIMO system. Based on the Bussgang decomposition, we reformulate the signal model with the nonlinear quantization operation as a statistically equivalent linear system.
- Then since the uplink-downlink duality is helpful when jointly design the precoder and receiver, we prove the uplink-downlink SINR duality in one-bit MIMO system at low operating region. On basis of the duality, we propose a new precoding scheme and downlink power allocation strategy, which make the uplink SINR can also be achieved in the downlink. In addition, we show that by using our proposed power allocation strategy, the dynamic range of the power amplifier is small, especially for the ZF precoding with large number of transmit antennas. We further observe that when achieving the same rate in the downlink transmission, the ZF precoding can use less power than the MF precoding.
- We quantify the theoretical rate achievable in both uplink and downlink using MRC/MF and ZF processing based on the LMMSE channel estimation. Closed-form expressions for the uplink and downlink achievable rate with MRC/MF and ZF processing are obtained as well, which enable us to look simultaneously at the uplink and downlink transmission to evaluate the system spectral efficiency and energy efficiency.
- By utilizing the multiple objective optimization framework, we investigate the optimal number of active terminals, pilot training length and system operating power to address the energy and spectral efficiency tradeoff problem. Clear tradeoff between EE and SE is observed in numerical results. In particular, we show that the power penalty in one-bit systems can be compensated for by deploying 2-2.5 times more antennas for MRC/MF processing, while for ZF processing, more and more antennas are required as SNR increases.

The rest of this paper is organized as follows. In next section, we present the assumed system architecture and signal model for both uplink and downlink. In Section III, we investigate the channel estimation and data transmission for one-bit MIMO systems by using the Bussgang decomposition. The uplink-downlink SINR duality in one-bit MIMO systems is proved in Section IV. In Section V, we provide approximate expressions for uplink and downlink achievable rate in one-bit massive MIMO systems. By employing the multiple objective optimization framework, we focus on the energy and spectral efficiency trade-off in Section VI, and investigate the optimal resource allocation to maximize both energy and spectral efficiency. Simulation results are presented in Section VI and we conclude the paper in Section VII.

Notation: The following notation is used throughout the paper. Bold uppercase (lowercase) letters denote matrices (vectors); $(.)^*$, $(.)^T$, and $(.)^H$ denote complex conjugate, transpose, and Hermitian transpose operations, respectively; $||.||$ represents the 2-norm of a vector; $\mathrm{tr}(.)$ represents the trace of a matrix; $\mathrm{diag}\{\mathbf{X}\}$ denotes a diagonal matrix containing only the diagonal entries of $\mathbf{X}$; $\otimes$ represents the Kronecker product; $[\mathbf{X}]_{ij}$ denotes the (i,j)th entry of $\mathbf{X}$; $\mathbf{x} \sim \mathcal{CN}(\mathbf{a}, \mathbf{B})$ indicates that $\mathbf{x}$ is a complex Gaussian vector with mean $\mathbf{a}$ and covariance matrix $\mathbf{B}$; $\mathrm{E}\{.\}$ and $\mathrm{Var}\{.\}$ denote the expected value and variance of a random variable, respectively.

II. System Model

As depicted in Fig. 1, we consider a single-cell massive

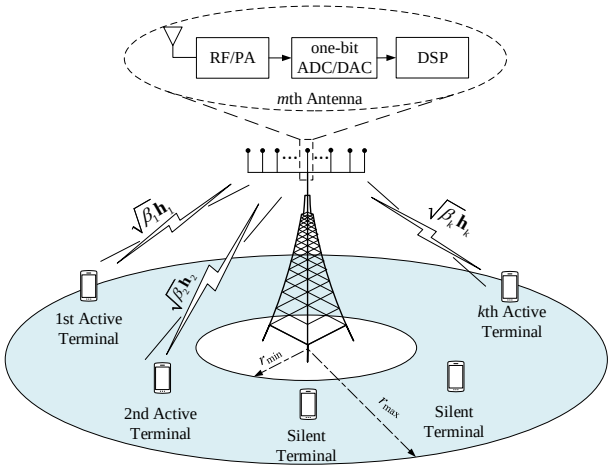

Fig. 1. System architecture of one-bit massive MIMO system.

MIMO system, where each antenna of the base station (BS) is assumed to be equipped with a pair of one-bit quantization devices. For the uplink transmission, the one-bit ADCs convert the real and imaginary part of the received signal from the analog domain, while for the downlink transmission, the one-bit DACs convert the precoded data symbols fed to the analog domain. We assume the BS is deployed with a large array of M antennas and communicates with K ($K \gg 1$) out of $K_{\max}$ single-antenna terminals at a time, where we refer to the K terminals as *active terminals* and to the remaining $K_{\max} - K$ as *silent terminals*. The K active terminals are randomly selected in a round-robin fashion, such that the subset of active terminals changes over time and hence, the index of the terminal $k \in \{1, ..., K\}$ corresponds to different terminals at different times. Therefore, the geographical position of the kth terminal is a random variable with a circular uniform distribution with maximum radius $r_{\max}$ and minimum radius $r_{\min}$. Let $\mathbf{g}_k \in \mathbb{C}^{M\times 1}$ denote the channel vector between the kth active terminal and the BS, which embraces independent fast fading, geometric attenuation and log-normal shadow fading and can be expressed as

$$\mathbf{g}_k = \sqrt{\beta_k}\mathbf{h}_k, \tag{1}$$

where $\mathbf{h}_k$ represents the fast fading channel of the kth active terminal and is assumed to be Gaussian distributed with zero mean and unit variance, while β_k is the large-scale fading coefficient to model both the geometric attenuation and shadow fading. Although the large scale fading coefficients of each antenna element can be modeled by using exact spherical wave model [25], in this paper we assume constant large fading coefficients across the antenna array since the distances between terminals and the BS are much larger than the antenna array length dimensions. More precisely, the large scale fading coefficient of the kth active terminal is modeled as

$$\beta_k = \frac{\bar{d}}{(d_k/r_{\min})^{\kappa}}, \tag{2}$$

where $\bar{d}$ is non-logarithmic shadowing value, κ is the path-loss exponent and d_k represents the distance between the kth user and the BS. Due to the slow-varying nature of the long term channel statistics, we assume large scale fading coefficients are known at the BS [1], [16].

In this paper, we assume that the one-bit massive MIMO system operates at time-division duplex (TDD) mode and the channels of the K active terminals satisfy the block fading assumption where the channel states stay constant over a coherence interval with a length of T symbols. Thus based on the reciprocal property of the uplink and downlink channels, the BS can process both uplink and downlink signals using the uplink channel measurement. In what follows, we define the uplink and downlink signal models for the one-bit MIMO system.

A. Uplink Signal Model

For the uplink transmission phase, we assume all the K active terminals simultaneously transmit independent data symbols to the BS. Thus the uplink received signal at the BS is

$$\mathbf{y}_{\mathrm{u}} = \sum_{k=1}^{K} \sqrt{p_k}\mathbf{g}_k s_k + \mathbf{n}_{\mathrm{u}}, \tag{3}$$

where the subscript 'u' stands for the 'uplink', p_k and s_k is the transmit power and transmit data symbol of the kth active terminal. In addition we assume $\mathrm{E}\{|s_k|^2\} = 1$ and $\mathrm{E}\{s_i s_k^H\} = 0$ for $i \neq k$. $\mathbf{n}_{\mathrm{u}} \sim \mathcal{CN}(0, \mathbf{I}) \in \mathbb{C}^{M\times 1}$ is additive white Gaussian noise. Then the uplink total transmit power can be given by $P_{\mathrm{total}}^{(\mathrm{UL})} = \sum_{k=1}^{K} p_k$.

In most existing literature, fixed and equal uplink transmit power for each active terminal is assumed. This may result in large rate disparity between the nearest and the furthest active terminals since the furthest active terminal suffers from the largest path attenuation. However, we consider statistic-aware power control strategy in this paper. That is to say the data symbols from the kth terminal have the transmit power of $p_k = \beta_k^{-1}\rho_{\mathrm{u}}$, where ρ_{u} is a system design parameter and we refer it as system *operating power* [12]. The quantized signal obtained after the one-bit ADCs is represented as

$$\begin{aligned}\mathbf{r}_{\mathrm{u}} = \mathcal{Q}(\mathbf{y}_{\mathrm{u}}) &= \mathcal{Q}\left(\sum_{k=1}^{K} \sqrt{p_k}\mathbf{g}_k s_k + \mathbf{n}_{\mathrm{u}}\right) \\ &= \mathcal{Q}\left(\sum_{k=1}^{K} \mathbf{g}_k^{\mathrm{eff}} s_k + \mathbf{n}_{\mathrm{u}}\right),\end{aligned} \tag{4}$$

where $\mathbf{g}_k^{\mathrm{eff}} = \sqrt{p_k}\mathbf{g}_k = \sqrt{\rho_{\mathrm{u}}}\mathbf{h}_k$ represents the effective power-controlled channel of the kth active terminal. Since the large scale fading coefficients can be compensated by adjusting the transmit power, we can model the effective channel as $\mathbf{g}_k^{\mathrm{eff}} \sim \mathcal{CN}(0, \rho_{\mathrm{u}}\mathbf{I})$, which implies that a uniform terminal experience can be guaranteed since each active terminal has the same channel statistics. $\mathcal{Q}(.)$ represents the one-bit quantization operation, which is applied separately to the real and imaginary part as $\mathcal{Q}(.) = \frac{1}{\sqrt{2}}(\mathrm{sign}(\Re(.)) + j\mathrm{sign}(\Im(.)))$. Thus, the output set of the one-bit quantization is equivalent to the quadrature phase-shift keying (QPSK) constellation points $\Omega = \frac{1}{\sqrt{2}}\{1 + j, 1 - j, -1 + j, -1 - j\}$.

B. Downlink Signal Model

For the downlink transmission phase, the BS forwards the precoded data symbols to the K active terminals simultaneously. We consider that the data symbols of the kth active terminal are precoded by a linear precoding vector $\mathbf{t}_k$ firstly. Then, going through the one-bit DACs at the BS, the real and imaginary part of the precoded signal are quantized from the digital domain to the analog domain. Therefore, the quantized analog signal can be expressed as

$$\mathbf{r}_{\mathrm{d}} = \mathcal{Q}\left(\mathbf{y}_{\mathrm{d}}\right) = \mathcal{Q}\left(\sum_{k=1}^{K} \mathbf{t}_k x_k\right). \tag{5}$$

where the subscript 'd' stands for 'downlink', x_k is the uncorrelated data symbols of the kth active terminal with zero mean and unit variance, which satisfies $\mathrm{E}\{|x_k|^2\} = 1$ and $\mathrm{E}\{x_i x_k^H\} = 0$ for $i \neq k$. Again, each element of $\mathbf{r}_{\mathrm{d}}$ lies in the set of Ω due to the one-bit quantization. As we assume that the system operates in TDD model, the received signal at the kth active terminal can be given by

$$\begin{aligned} u_{\mathrm{d},k} &= \mathbf{g}_k^T \mathbf{Q} \mathbf{r}_{\mathrm{d}} + n_{\mathrm{d},k} \\ &= \mathbf{g}_k^T \mathbf{Q} \mathcal{Q}\left(\sum_{k=1}^{K} \mathbf{t}_k x_k\right) + n_{\mathrm{d},k}, \end{aligned} \tag{6}$$

where $n_{\mathrm{d},k}$ is the additive white Gaussian noise received at the kth active terminal. $\mathbf{Q}$ is a diagonal matrix represents the power allocation of each BS antenna, and hence the total transmission power of the downlink is $P_{\mathrm{total}}^{(\mathrm{DL})} = \mathrm{tr}\left(\mathbf{Q}\mathbf{Q}^H\right)$.

Note that contrary to the conventional MIMO systems, where the transmit power allocation can be considered jointly with the precoding vector, transmit power allocation of each BS antenna should be considered separately in one-bit MIMO systems since the power of each element of the output signal $\mathbf{y}_{\mathrm{d}}$ is normalized due to the one-bit quantization. Any power control can be considered in the downlink since the BS has access to the estimated CSI. We later show how to design the precoding vector $\mathbf{t}_k$ and transmit power matrix $\mathbf{Q}$ to achieve the same achievable rate performance in the downlink as in the uplink.

III. Channel Estimation and Data Transmission for One-Bit MIMO Systems

During the period of communication between the K active terminals and the BS, we assume the channels satisfy the block fading with coherence interval of T. In the TDD transmission mode, we also assume each coherence interval block is divided into three parts: First the $\tau = \tau_0 K$ symbols reserved for pilot training with arbitrary positive relative pilot $\tau_0 \geq 1$ and $\tau \in \mathbb{R}_+$, then the remaining $T - \tau$ symbols are split into uplink and downlink data transmission phase. We denote $\gamma \in (0, 1)$ as the coherence interval fraction factor allocated for uplink transmission and $1-\gamma$ for downlink transmission. The fraction factor can be selected arbitrarily to make sure $\gamma(T - \tau)$ is a positive integer.

A. Channel Estimation

In a standard implementation, the CSI is estimated at the BS by pilot training. During training, we assume all K users simultaneously transmit their pilot sequences of τ symbols each to the BS, which yields

$$\mathbf{Y}_{\mathrm{t}} = \sum_{k=1}^{K} \sqrt{p_k} \mathbf{g}_k \boldsymbol{\phi}_k^T + \mathbf{N}_{\mathrm{t}} = \sum_{k=1}^{K} \mathbf{g}_k^{\mathrm{eff}} \boldsymbol{\phi}_k^T + \mathbf{N}_{\mathrm{t}}, \tag{7}$$

where the subscript 't' stands for 'training', $\mathbf{Y}_{\mathrm{t}} \in \mathbb{C}^{M \times \tau}$ is the received training signal matrix, p_k and $\boldsymbol{\phi}_k \in \mathbb{C}^{\tau \times 1}$ are the pilot transmit power and the pilot sequences of the kth user, respectively. In this paper, all pilot sequences are assumed to be mutual orthogonal, i.e., $\boldsymbol{\phi}_k^T \boldsymbol{\phi}_k^* = \tau$ and $\boldsymbol{\phi}_i^T \boldsymbol{\phi}_k^* = 0$ for $i \neq k$.

To match the matrix form of (7) to the vector form of (4), we vectorize the received signal as

$$\mathbf{y}_{\mathrm{t}} = \mathrm{vec}(\mathbf{Y}_{\mathrm{t}}) = \sum_{k=1}^{K} \bar{\boldsymbol{\phi}}_k \mathbf{g}_k^{\mathrm{eff}} + \mathbf{n}_{\mathrm{t}}, \tag{8}$$

where $\bar{\boldsymbol{\phi}}_k = (\boldsymbol{\phi}_k \otimes \mathbf{I}_M)$, $\mathbf{n}_{\mathrm{t}} = \mathrm{vec}(\mathbf{N}_{\mathrm{t}})$. After one-bit ADCs, the quantized signal can be expressed as

$$\mathbf{r}_{\mathrm{t}} = \mathcal{Q}(\mathbf{y}_{\mathrm{t}}) = \mathcal{Q}\left(\sum_{k=1}^{K} \bar{\boldsymbol{\phi}}_k \mathbf{g}_k^{\mathrm{eff}} + \mathbf{n}_{\mathrm{t}}\right), \tag{9}$$

where each element of $\mathbf{r}_{\mathrm{t}}$ takes values from the set Ω. We would like to remark that the output of (9), $\mathbf{r}_{\mathrm{t}}$, is totally independent of any real scaling factor applied to $\mathbf{y}_{\mathrm{t}}$. Using the Bussgang decomposition [26], we can reformulate the nonlinear quantization with a statistically equivalent linear operator that will simplify the channel estimator and the resulting analysis. In particular, for the quantized signal (9), the Bussgang decomposition is written

$$\mathbf{r}_{\mathrm{t}} = \mathcal{Q}(\mathbf{y}_{\mathrm{t}}) = \mathbf{A}_{\mathrm{t}} \mathbf{y}_{\mathrm{t}} + \boldsymbol{\eta}_{\mathrm{t}} = \sum_{k=1}^{K} \tilde{\boldsymbol{\phi}}_k \mathbf{g}_k^{\mathrm{eff}} + \tilde{\mathbf{n}}_{\mathrm{t}}, \tag{10}$$

where $\tilde{\boldsymbol{\phi}}_k = \mathbf{A}_{\mathrm{t}} \bar{\boldsymbol{\phi}}_k$ and $\tilde{\mathbf{n}}_{\mathrm{t}} = \mathbf{A}_{\mathrm{t}} \mathbf{n}_{\mathrm{t}} + \boldsymbol{\eta}_{\mathrm{t}}$ is the effective noise. $\mathbf{A}_{\mathrm{t}}$ is a given matrix and $\boldsymbol{\eta}_{\mathrm{t}}$ the statistically equivalent quantization noise. The matrix $\mathbf{A}_{\mathrm{t}}$ is chosen to make $\boldsymbol{\eta}_{\mathrm{t}}$ uncorrelated with $\mathbf{y}_{\mathrm{t}}$ [26], or equivalently, to minimize the power of the equivalent quantization noise. This yields [8]

$$\begin{aligned} \mathbf{A}_{\mathrm{t}} &= \sqrt{\frac{2}{\pi}} \mathrm{diag}\left(\mathbf{C}_{\mathbf{y}_{\mathrm{t}}}\right)^{-\frac{1}{2}} \\ &= \sqrt{\frac{2}{\pi}} \mathrm{diag}\left(\sum_{k=1}^{K} \rho_{\mathrm{u}} (\boldsymbol{\phi}_k \boldsymbol{\phi}_k^H \otimes \mathbf{I}_M) + \mathbf{I}_{M\tau}\right)^{-\frac{1}{2}}, \end{aligned} \tag{11}$$

where $\mathbf{C}_{\mathbf{y}_{\mathrm{t}}}$ denotes the covariance matrix of $\mathbf{y}_{\mathrm{t}}$.

We can see from (11) that, $\mathbf{A}_{\mathrm{t}}$ is related to the diagonal terms of $\mathbf{C}_{\mathbf{y}_{\mathrm{t}}}$ and therefore, to the pilot sequences. In order to obtain a simple expression for $\mathbf{A}_{\mathrm{t}}$, we consider pilot sequences composed of submatrices of the discrete Fourier transform (DFT) operator [27]. The benefits of using DFT pilot sequences are: i) all the elements of the matrix have the same magnitude, which simplifies peak transmit power constraints, and ii) the diagonal terms of $\boldsymbol{\phi}_k \boldsymbol{\phi}_k^H$ are always equals to 1,

which results in a simple expression for $\mathbf{A}_{\mathrm{t}}$, as follows:

$$\mathbf{A}_{\mathrm{t}} = \sqrt{\frac{2}{\pi}\frac{1}{K\rho_{\mathrm{u}}+1}}\mathbf{I} = \alpha\mathbf{I}. \tag{12}$$

Since the one-bit quantization results in a new signal $\mathbf{r}_{\mathrm{t}}$ with unit variance, the individual transmit power p_k of each user is hard to be estimated [28]. Therefore we estimate the effective channels $\mathbf{g}_k^{\mathrm{eff}}$ including the uplink power-control, instead of the true channel $\mathbf{g}_k$. In this way, we can estimate the channel without taking the transmit power p_k into account. According to [29] and the fact that $\boldsymbol{\eta}_p$ is uncorrelated with the channel $\mathbf{g}_k^{\mathrm{eff}}$ (See detail proof in [8]), the LMMSE channel estimate of $\mathbf{g}_k^{\mathrm{eff}}$ can be expressed as

$$\hat{\mathbf{g}}_k^{\mathrm{eff}} = \tilde{\boldsymbol{\phi}}_k^H \mathbf{C}_{\mathbf{r}_{\mathrm{t}}}^{-1}\mathbf{r}_{\mathrm{t}}, \tag{13}$$

where $\mathbf{C}_{\mathbf{r}_{\mathrm{t}}}$ is the auto-correlation matrix of $\mathbf{r}_{\mathrm{t}}$. It has been shown in [30] that for one-bit ADCs, the arcsin law can be used to obtain $\mathbf{C}_{\mathbf{r}_{\mathrm{t}}}$:

$$\begin{aligned}\mathbf{C}_{\mathbf{r}_{\mathrm{t}}} =& \frac{2}{\pi}\left(\arcsin\left(\boldsymbol{\Sigma}_{\mathbf{y}_{\mathrm{t}}}^{-\frac{1}{2}}\Re\left(\mathbf{C}_{\mathbf{y}_{\mathrm{t}}}\right)\boldsymbol{\Sigma}_{\mathbf{y}_{\mathrm{t}}}^{-\frac{1}{2}}\right)\right.\\ &\left.+j\arcsin\left(\boldsymbol{\Sigma}_{\mathbf{y}_{\mathrm{t}}}^{-\frac{1}{2}}\Im\left(\mathbf{C}_{\mathbf{y}_{\mathrm{t}}}\right)\boldsymbol{\Sigma}_{\mathbf{y}_{\mathrm{t}}}^{-\frac{1}{2}}\right)\right).\end{aligned} \tag{14}$$

where we define $\boldsymbol{\Sigma}_{\mathbf{y}_{\mathrm{t}}} = \mathrm{diag}\left(\mathbf{C}_{\mathbf{y}_{\mathrm{t}}}\right)$. The covariance matrix of the estimation error $\boldsymbol{\varepsilon}_k^{\mathrm{eff}} = \mathbf{g}_k^{\mathrm{eff}} - \hat{\mathbf{g}}_k^{\mathrm{eff}}$ is given by

$$\begin{aligned}\mathbf{C}_{\boldsymbol{\varepsilon}_k^{\mathrm{eff}}} &= \mathrm{E}\left\{\left(\mathbf{g}_k^{\mathrm{eff}} - \hat{\mathbf{g}}_k^{\mathrm{eff}}\right)\left(\mathbf{g}_k^{\mathrm{eff}} - \hat{\mathbf{g}}_k^{\mathrm{eff}}\right)^H\right\}\\ &= \rho_{\mathrm{u}}\mathbf{I}_M - \tilde{\boldsymbol{\phi}}_k^H\mathbf{C}_{\mathbf{r}_{\mathrm{t}}}^{-1}\tilde{\boldsymbol{\phi}}_k\end{aligned} \tag{15}$$

and the mean-squared error (MSE) is $\mathrm{MSE}_k = \mathrm{tr}(\mathbf{C}_{\boldsymbol{\varepsilon}_k^{\mathrm{eff}}})$.

Note that, it is obvious that $\mathbf{C}_{\mathbf{y}_{\mathrm{t}}}$ is a circulant matrix, $\mathbf{C}_{\mathbf{r}_{\mathrm{t}}}$ is also a circulant matrix since "arcsin" is an element-wise operation. According to [31], the inverse of a circulant matrix is still a circulant matrix, which can be diagonalized by a DFT matrix. Therefore, another advantage of using the DFT matrix as the pilot sequences is that, by using the channel estimator in (13), the elements of the channel estimate are mutual uncorrelated. Thus, the covariance matrix of the estimation error in (15) is diagonal, which implies that the elements of the channel estimate error are uncorrelated.

B. Data Transmission

During the data transmission phase, the BS considers the channel estimates as the true channel and employs linear processing techniques to process the data symbols in the digital domain. More precisely, the BS first uses a linear receiver to decode the signals transmitted from the K active terminals in the uplink and then uses linear precoding vectors to broadcast the signals to the K active terminals in the downlink.

1) Linear Receiver: In the uplink transmission, we assume the K users simultaneously transmit their data symbols to the BS. We again employ the Bussgang decomposition and reformulate the nonlinear quantizer $\mathcal{Q}(.)$ as a linear function, and the quantized signal at the BS can be expressed as

$$\begin{aligned}\mathbf{r}_{\mathrm{u}} = \mathcal{Q}(\mathbf{y}_{\mathrm{u}}) &= \mathcal{Q}\left(\sum_{k=1}^{K}\sqrt{p_k}\mathbf{g}_k s_k + \mathbf{n}_{\mathrm{u}}\right)\\ &= \mathbf{A}_{\mathrm{u}}\sum_{k=1}^{K}\mathbf{g}_k^{\mathrm{eff}}s_k + \mathbf{A}_{\mathrm{u}}\mathbf{n}_{\mathrm{u}} + \boldsymbol{\eta}_{\mathrm{u}},\end{aligned} \tag{16}$$

where the same definitions as in the previous sections apply, but replacing the subscript 't' with 'u'. Again, according to the Bussgang decomposition, the matrix of $\mathbf{A}_{\mathrm{u}}$ for Gaussian input can be given by

$$\begin{aligned}\mathbf{A}_{\mathrm{u}} &= \sqrt{\frac{2}{\pi}}\mathrm{diag}\left(\mathbf{C}_{\mathbf{y}_{\mathrm{u}}}\right)^{-\frac{1}{2}}\\ &= \sqrt{\frac{2}{\pi}}\mathrm{diag}\left(\sum_{k=1}^{K}\mathbf{g}_k^{\mathrm{eff}}(\mathbf{g}_k^{\mathrm{eff}})^H + \mathbf{I}_M\right)^{-\frac{1}{2}}\\ &\cong \sqrt{\frac{2}{\pi}}\sqrt{\frac{1}{K\rho_{\mathrm{u}}+1}}\mathbf{I}_M = \alpha\mathbf{I}_M,\end{aligned} \tag{17}$$

where the approximation is reasonable since we assume $K \gg 1$ and i.i.d. effective channel coefficients.

Note that different with (11), where the pilot sequences are fixed and the expectation operation are taken over channel vectors, the expectation in (17) is taken over the data symbols for each individual channel realization. In this way, the effect that the quantization noise sometimes appears to coherently combine with the data symbols showed in [9] can be avoided.

With linear receiver, the quantized signal $\mathbf{r}_{\mathrm{u}}$ is separated into K streams by multiplying it with a linear receiver matrix $\mathbf{W}^T$ as follows:

$$\begin{aligned}\hat{\mathbf{s}} &= \mathbf{W}^T\mathbf{r}_{\mathrm{u}}\\ &= \mathbf{W}^T\mathbf{A}_{\mathrm{u}}\sum_{k=1}^{K}\mathbf{g}_k^{\mathrm{eff}}s_k + \mathbf{W}^T\mathbf{A}_{\mathrm{u}}\mathbf{n}_{\mathrm{u}} + \mathbf{W}^T\boldsymbol{\eta}_{\mathrm{u}},\end{aligned} \tag{18}$$

Then the kth stream is used to decode the signal transmitted from the kth active terminal, which can be expressed as

$$\begin{aligned}\hat{s}_k =& \mathbf{w}_k^T\mathbf{A}_{\mathrm{u}}\mathbf{g}_k^{\mathrm{eff}}s_k + \mathbf{w}_k^T\sum\nolimits_{i\neq k}^{K}\mathbf{A}_{\mathrm{u}}\mathbf{g}_i^{\mathrm{eff}}s_i\\ &+ \mathbf{w}_k^T\mathbf{A}_{\mathrm{u}}\mathbf{n}_{\mathrm{u}} + \mathbf{w}_k^T\boldsymbol{\eta}_{\mathrm{u}},\end{aligned} \tag{19}$$

where $\mathbf{w}_k$ is the kth columns of $\mathbf{W}$. The last three terms in (19) respectively correspond to user interference, AWGN noise and quantization noise.

2) Linear Precoding: In the downlink transmission phase, similar with the uplink transmission, we can reformulate the precoded signal model of (5) using the Bussgang decomposition, yields

$$\mathbf{r}_{\mathrm{d}} = \mathcal{Q}\left(\sum_{k=1}^{K}\mathbf{t}_k x_k\right) = \mathbf{A}_{\mathrm{d}}\sum_{k=1}^{K}\mathbf{t}_k x_k + \boldsymbol{\eta}_{\mathrm{d}}, \tag{20}$$

where the same definitions as in the previous sections apply, but replacing the subscript t with d. The matrix of $\mathbf{A}_{\mathrm{d}}$ for Gaussian input is given by

$$\mathbf{A}_{\mathrm{d}} = \sqrt{\frac{2}{\pi}}\mathrm{diag}\left(\mathbf{C}_{\mathbf{y}_{\mathrm{d}}}\right)^{-\frac{1}{2}} = \sqrt{\frac{2}{\pi}}\mathrm{diag}\left(\sum_{k=1}^{K}\mathbf{t}_k\mathbf{t}_k^H\right)^{-\frac{1}{2}}. \tag{21}$$

Substituting (20) into (6), the received signal at the kth terminal can be expressed as

$$u_{\mathrm{d},k} = \mathbf{g}_k^T \mathbf{Q} \mathcal{Q}\left(\sum_{k=1}^{K} \mathbf{t}_k x_k\right) + n_{\mathrm{d},k}$$
$$= \mathbf{g}_k^T \mathbf{Q}\mathbf{A}_{\mathrm{d}} \mathbf{t}_k x_k + \mathbf{g}_k^T \mathbf{Q}\mathbf{A}_{\mathrm{d}} \sum_{i\neq k}^{K} \mathbf{t}_i x_i + \mathbf{g}_k^T \mathbf{Q}\boldsymbol{\eta}_{\mathrm{d}} + n_{\mathrm{d},k}. \quad (22)$$

The last three terms in (22) respectively correspond to multiuser interference, quantization noise and AWGN noise.

IV. Uplink-Downlink SINR Duality in One-Bit MIMO Systems

From a network operator's perspective, it is necessary to fulfill individual target signal-to-interference-plus-noise ratio (SINR), which depends on the choice of receiver/precoder and transmit power, for both successful uplink and downlink communication. Generally, the receiver and precoder can be designed in a variety of ways to satisfy the specific uplink and downlink SINR. However, it is more difficult to optimize a precoder than a receiver in general, the uplink-downlink SINR duality theorem is a key tool which simplify substantially the problem of joint design of precoder and receiver. In fact, the duality between the downlink (broadcast) and the uplink (multiple access) of the unquantized MIMO systems has been proved in many previous works [32]. However, for quantized MIMO systems, especially for one-bit MIMO systems, the uplink-downlink SINR duality has not been proved. Therefore, in this paper, we assume both uplink and downlink use the same type of processing vectors and find the conditions for the uplink and downlink duality holds in one-bit systems. As we will see later, this uplink-downlink duality allows us to derive the EE-SE tradeoff, which is valid for both links.

According to the signal model of (19) and (22) we provided in previous section, the individual uplink and downlink SINR of the kth active user can be expressed as (23) and (24) shown in the top of next page, where the matrix of $\mathbf{C}_{\boldsymbol{\eta}_{\mathrm{p}}}$ denotes the covariance matrix of the quantizer noise $\boldsymbol{\eta}_{\mathrm{p}}$ and given by

$$\mathbf{C}_{\boldsymbol{\eta}_{\mathrm{p}}} = \mathbf{C}_{\mathbf{r}_{\mathrm{p}}} - \mathbf{A}_{\mathrm{p}} \mathbf{C}_{\mathbf{y}_{\mathrm{p}}} \mathbf{A}_{\mathrm{p}}^H, \quad (25)$$

where the subscript 'p' stands for 'phase' and belongs to the set of $\mathrm{p} \in \{\mathrm{t}, \mathrm{u}, \mathrm{d}\}$. According to the arcsin law, which states that for one-bit quantization the covariance of the quantizer output can be obtained by that of the input, we can rewrite the covariance matrix of the quantizer noise $\boldsymbol{\eta}_{\mathrm{p}}$ as

$$\mathbf{C}_{\boldsymbol{\eta}_{\mathrm{p}}} = \frac{2}{\pi}(\arcsin(\mathbf{X}_{\mathrm{p}}) + j \arcsin(\mathbf{Y}_{\mathrm{p}})) - \frac{2}{\pi}(\mathbf{X}_{\mathrm{p}} + j\mathbf{Y}_{\mathrm{p}}), \quad (26)$$

where we define the matrix of $\mathbf{X}_{\mathrm{p}}$ and $\mathbf{Y}_{\mathrm{p}}$ as

$$\mathbf{X}_{\mathrm{p}} = \mathrm{diag}(\mathbf{C}_{\mathbf{y}_{\mathrm{p}}})^{-\frac{1}{2}} \Re\left(\mathbf{C}_{\mathbf{y}_{\mathrm{p}}}\right) \mathrm{diag}(\mathbf{C}_{\mathbf{y}_{\mathrm{p}}})^{-\frac{1}{2}}, \quad (27)$$
$$\mathbf{Y}_{\mathrm{p}} = \mathrm{diag}(\mathbf{C}_{\mathbf{y}_{\mathrm{p}}})^{-\frac{1}{2}} \Im\left(\mathbf{C}_{\mathbf{y}_{\mathrm{p}}}\right) \mathrm{diag}(\mathbf{C}_{\mathbf{y}_{\mathrm{p}}})^{-\frac{1}{2}}. \quad (28)$$

The 'arcsin' function is a nonlinear and element-wise operation, and hence, it is complicated to prove the SINR duality directly. However, it is expected that massive MIMO systems will operate at low operating power region due to the availability of a large array gain. In what follows, we show that using a low power operating assumption allows us to derive an approximation of the arcsin operation:

$$\frac{2}{\pi}\arcsin(a) \cong \begin{cases} 1, & a = 1 \\ 2a/\pi, & a < 1 \end{cases} \quad (29)$$

Since the non-elements of the $\mathbf{X}_{\mathrm{p}}$ and $\mathbf{Y}_{\mathrm{p}}$ are far smaller than 1 in the low operating power region, we can approximate (26) as

$$\mathbf{C}_{\boldsymbol{\eta}_{\mathrm{p}}} \cong (1 - 2/\pi)\mathbf{I}. \quad (30)$$

By using this approximation, we provide Theorem 1 next.

Theorem 1: For one-bit MIMO system at low operating region, there exist a linear precoding scheme with $\mathbf{t}_i = \mathbf{A}_{\mathrm{u}}\mathbf{w}_i$ and downlink power allocation strategy with

$$\mathbf{Q} = \sqrt{\frac{\pi}{2}}\mathrm{diag}\left(\sum_{i=1}^{K} \mathbf{t}_i \mathbf{t}_i^H\right)^{\frac{1}{2}}, \quad (31)$$

to make sure the SINR achieved in the uplink can be also achieved in the downlink, yields:

$$\mathrm{SINR}_k^{(\mathrm{UL})} = \mathrm{SINR}_k^{(\mathrm{DL})}. \quad (32)$$

Proof: See proof in Appendix A. ∎

Next we will use Theorem 1 to analyze the achievable rate by simultaneously considering the uplink and downlink transmission.

V. Achievable Rate Approximation in One-Bit Massive MIMO Systems

In one-bit MIMO system, the quantizer noise for both uplink and downlink is not Gaussian due to the one-bit quantization. However the entropy of the uncorrelated effective noise is upper-bounded by the entropy of Gaussian noise, and this minimizes the mutual information of the input and output [33]. Therefore, a lower bound for the achievable rate can be found by modeling the quantizer noise $\boldsymbol{\eta}_{\mathrm{u}}$ and $\boldsymbol{\eta}_{\mathrm{d}}$ as Gaussian with the same covariance matrix shown in (25). Thus the ergodic achievable rate for both uplink and downlink transmission in one-bit MIMO system is lower bounded by

$$\tilde{R}_k^{(\mathrm{Link})} = \mathrm{E}\left\{\log_2\left(1 + \mathrm{SINR}_k^{(\mathrm{Link})}\right)\right\}, \quad (33)$$

where $\mathrm{Link} \in \{\mathrm{UL}, \mathrm{DL}\}$, and $\mathrm{SINR}_k^{(\mathrm{UL})}$ and $\mathrm{SINR}_k^{(\mathrm{DL})}$ are shown in (23) and (24), respectively [16]. As mentioned before, the massive MIMO system is expected to operate at low operating power due to availability of the large antenna gain. Therefore, in this section we mainly focus on deriving the closed-form expression of the achievable rate in the low operating power region.

Before we proceed, we first focus on deriving an approximation of the channel estimation. The covariance matrix of the estimate effective channel $\hat{\mathbf{g}}_k^{\mathrm{eff}}$ (13) is given by

$$\mathbf{C}_{\hat{\mathbf{g}}_k^{\mathrm{eff}}} = \tilde{\boldsymbol{\phi}}_k^H \mathbf{C}_{\mathbf{r}_{\mathrm{t}}} \tilde{\boldsymbol{\phi}}_k. \quad (34)$$

We see that the expression above involves the covariance matrix $\mathbf{C}_{\mathbf{r}_{\mathrm{t}}}$, which is complicated due to the arcsin law of (14). However, by using the approximation of (29) in the low operating power region and using the linear form of $\mathbf{r}_{\mathrm{t}}$ shown

$$\mathrm{SINR}_k^{(\mathrm{UL})} = \frac{p_k|\mathbf{w}_k^T\mathbf{A}_{\mathrm{u}}\mathbf{g}_k|^2}{\sum_{i\neq k}^{K} p_i|\mathbf{w}_k^T\mathbf{A}_{\mathrm{u}}\mathbf{g}_i|^2 + \|\mathbf{w}_k^T\mathbf{A}_{\mathrm{u}}\|_2^2 + \mathbf{w}_k^T\mathbf{C}_{\boldsymbol{\eta}_{\mathrm{u}}}\mathbf{w}_k^*}, \tag{23}$$

$$\mathrm{SINR}_k^{(\mathrm{DL})} = \frac{|\mathbf{g}_k^T\mathbf{Q}\mathbf{A}_{\mathrm{d}}\mathbf{t}_k|^2}{\sum_{i\neq k}^{K} |\mathbf{g}_k^T\mathbf{Q}\mathbf{A}_{\mathrm{d}}\mathbf{t}_i|^2 + \mathbf{g}_k^T\mathbf{Q}\mathbf{C}_{\boldsymbol{\eta}_{\mathrm{d}}}\mathbf{Q}^H\mathbf{g}_k^* + 1}. \tag{24}$$

in (10), the covariance matrix of $\mathbf{C}_{\boldsymbol{\eta}_{\mathrm{t}}}$ can be approximated as

$$\begin{aligned}\mathbf{C}_{\mathbf{r}_{\mathrm{t}}} &= \sum_{k=1}^{K}\rho\tilde{\boldsymbol{\phi}}_k\tilde{\boldsymbol{\phi}}_k^H + \mathbf{A}_{\mathrm{t}}\mathbf{A}_{\mathrm{t}}^H + \mathbf{C}_{\boldsymbol{\eta}_{\mathrm{t}}\boldsymbol{\eta}_{\mathrm{t}}} \\ &\cong \sum_{k=1}^{K}\rho_{\mathrm{u}}\tilde{\boldsymbol{\phi}}_k\tilde{\boldsymbol{\phi}}_k^H + (\alpha^2 + 1 - \frac{2}{\pi})\mathbf{I}, \end{aligned}\tag{35}$$

since the covariance matrix $\mathbf{C}_{\boldsymbol{\eta}_{\mathrm{t}}}$ of the quantizer noise $\boldsymbol{\eta}_{\mathrm{t}}$ can be approximated as an identity matrix with a scaling factor $1 - 2/\pi$.

Note that, although the elements of the channel estimate (13) are not exactly distributed as Gaussian due to the one-bit quantization, we can approximate it as Gaussian according to Cramér's central limit theorem [34] since each element of $\hat{\mathbf{g}}_k^{\mathrm{eff}}$ can be expressed as a summation of a large number of random variables. Therefore, in the sequel each element of the channel estimate $\hat{\mathbf{g}}_k^{\mathrm{eff}}$ can be approximated as Gaussian with covariance matrix of

$$\begin{aligned}\mathbf{C}_{\hat{\mathbf{g}}_k^{\mathrm{eff}}} &\cong \tilde{\boldsymbol{\phi}}_k^H\left(\sum_{k=1}^{K}\rho_{\mathrm{u}}\tilde{\boldsymbol{\phi}}_k\tilde{\boldsymbol{\phi}}_k^H + \left(\alpha^2 + 1 - \frac{2}{\pi}\right)\mathbf{I}\right)^{-1}\tilde{\boldsymbol{\phi}}_k \\ &= \frac{\alpha^2\tau\rho_{\mathrm{u}}^2}{\alpha^2\tau\rho_{\mathrm{u}} + \alpha^2 + 1 - 2/\pi}\mathbf{I} = \sigma^2\mathbf{I}, \end{aligned}\tag{36}$$

which implies that, in the low operating power region, each element of the channel estimate $\hat{\mathbf{g}}_k^{\mathrm{eff}}$ can be approximated as independent and identically Gaussian distributed (i.i.d) with zero mean and variance of σ^2.

A. Uplink Transmission

In this subsection we focus on deriving the closed-form expression for uplink achievable rate. Since there is no efficient way to directly calculate the achievable rate in (33), we borrow Lemma 1 from [35] to derive an approximate closed-form expression of the achievable rate. For completeness and convenience, we provide it in the following.

Lemma 1: If $X = \sum_{i=1}^{M} X_i$ and $Y = \sum_{i=j}^{M} Y_j$ are both sums of nonnegative random variables X_i and Y_j, then we get the following approximation

$$\mathrm{E}\left\{\log_2\left(1 + \frac{X}{Y}\right)\right\} \cong \log_2\left(1 + \frac{\mathrm{E}\{X\}}{\mathrm{E}\{Y\}}\right). \tag{37}$$

Proof: See detail proof in [35]. ■

Note that the approximation in Lemma 1 does not require the random variables X and Y to be independent and becomes more accurate as M increase. Thus, in massive MIMO configuration, due to the large number of BS antennas, this approximation will be particularly accurate [35].

According to Lemma 1 and substituting $\mathbf{A}_{\mathrm{u}} = \alpha\mathbf{I}$, we can approximate the uplink ergodic achievable rate $\tilde{R}_k^{(\mathrm{UL})}$ by

$$R_k^{(\mathrm{UL})} = \log_2\left(1 + \frac{\alpha^2\mathrm{E}\left\{\left|\mathbf{w}_k^T\mathbf{g}_k^{\mathrm{eff}}\right|^2\right\}}{\sum_{i\neq k}^{K}\alpha^2\mathrm{E}\left\{\left|\mathbf{w}_k^T\mathbf{g}_i^{\mathrm{eff}}\right|^2\right\} + \mathrm{AQN}_k}\right), \tag{38}$$

where we define

$$\mathrm{AQN}_k = \alpha^2\mathrm{E}\left\{\left\|\mathbf{w}_k^T\right\|_2^2\right\} + \mathrm{E}\left\{\mathbf{w}_k^T\mathbf{C}_{\boldsymbol{\eta}_{\mathrm{u}}}\mathbf{w}_k^*\right\}, \tag{39}$$

and the expectation operation is taken with respect to the channel realizations. In this paper, we will consider the performance of the usual MRC and ZF receiver, defined by

$$\mathbf{W}_{\mathrm{MRC}}^T = \hat{\mathbf{G}}_{\mathrm{eff}}^H \tag{40}$$

$$\mathbf{W}_{\mathrm{ZF}}^T = \left(\hat{\mathbf{G}}_{\mathrm{eff}}^H\hat{\mathbf{G}}_{\mathrm{eff}}^H\right)^{-1}\hat{\mathbf{G}}_{\mathrm{eff}}^H \tag{41}$$

respectively, where $\hat{\mathbf{G}}_{\mathrm{eff}} = \left[\hat{\mathbf{g}}_1^{\mathrm{eff}}, ..., \hat{\mathbf{g}}_K^{\mathrm{eff}}\right]$. We next provide approximate closed-form expressions for the uplink achievable rate given by (33) for MRC and ZF receiver.

Theorem 2: For an MRC receiver based on the LMMSE channel estimate and in low operating power region, the uplink achievable rate of each active terminal in one-bit massive MIMO system can be approximated by

$$R_{\mathrm{MRC}}^{(\mathrm{UL})} = \log_2\left(1 + \frac{\alpha^2(\sigma^2 M + \rho_{\mathrm{u}})}{\rho_{\mathrm{u}}\alpha^2(K-1) + \alpha^2 + 1 - 2/\pi}\right), \tag{42}$$

Proof: See detail proof in Appendix B. ■

Theorem 3: For ZF receiver based on the LMMSE channel estimate and in the low operating power region, the uplink achievable rate of each active terminal in one-bit massive MIMO system can be approximated by

$$R_{\mathrm{ZF}}^{(\mathrm{UL})} = \log_2\left(1 + \frac{\alpha_{\mathrm{u}}^2\sigma^2(M-K-1) + \alpha_{\mathrm{u}}^2\rho_{\mathrm{u}}}{\alpha_{\mathrm{u}}^2(K-1)(\rho_{\mathrm{u}} - \sigma^2) + \alpha_{\mathrm{u}}^2 + 1 - 2/\pi}\right), \tag{43}$$

Proof: See detail proof in Appendix C. ■

Note that equal achievable rate can be guaranteed to all active terminals due to the power control strategy, thus we omit the subscript k in the achievable rate of (42) and (43).

B. Downlink Transmission

In the downlink transmission for conventional MIMO system[1], in order to satisfy the uplink-downlink duality, the precoding vectors are often assumed to be $\mathbf{t}_k = \sqrt{q_k/\|\mathbf{w}_k\|^2}\mathbf{w}_k$, where the scaling factor of $\sqrt{q_k/\|\mathbf{w}_k\|^2}$ is chosen to satisfy the total transmit power constraint such that the total transmission power of the uplink and downlink are equal. However, according to Theorem 1, in contrast to the conventional MIMO

[1]Conventional MIMO systems are assumed to be equipped with perfect hardware with infinite-resolution level of ADC/DACs.

systems, the scaling factor $\sqrt{q_k/\|\mathbf{w}_k\|^2}$ is replaced by the scaling matrix $\mathbf{A}_{\rm u}$ in one-bit systems to make sure the duality holds. That is to say, although the power of the quantization output $\mathbf{r}_{\rm d}$ does not change with $\mathbf{t}_k$ and it seems that the power allocation is done for each antenna instead of each user, in fact the power is allocated to different users by using the precoding scheme $\mathbf{t}_k = \mathbf{A}_{\rm u}\mathbf{w}_k$.Therefore in what follows, we consider new matched-filter (MF) and ZF precoding schemes shown as

$$\mathbf{T}_{\rm MF} = \mathbf{A}_{\rm u}\hat{\mathbf{G}}^*_{\rm eff}, \tag{44}$$

$$\mathbf{T}_{\rm ZF} = \mathbf{A}_{\rm u}\hat{\mathbf{G}}^*_{\rm eff}\left(\hat{\mathbf{G}}^T_{\rm eff}\hat{\mathbf{G}}^*_{\rm eff}\right)^{-1}. \tag{45}$$

Then we evaluate the downlink achievable rate for the two new precoding strategies and provide the following theorem.

Theorem 4: In one-bit MIMO systems, by employing the precoding strategies shown in (44) and (45) and allocating transmit power with

$$\mathbf{Q} = \sqrt{\frac{\pi}{2}}{\rm diag}\left(\mathbf{T}\mathbf{T}^H\right)^{\frac{1}{2}}, \tag{46}$$

the ergodic downlink achievable rate of each active terminal can be approximated by (42) and (43), respectively.

Proof: This follows directly from the uplink-downlink SINR duality for one-bit MIMO system in Theorem 1. ■

Next we will investigate the optimal system design parameters for fixed M and T on basis of the closed-form expression of the uplink and downlink achievable rate.

VI. Optimal System Design of EE-SE Tradeoff for One-Bit Massive MIMO

Generally in most existing literature, the system performance of spectral or energy efficiency is optimized separately, such that one of the objective is of dominating importance and the system sets desirable values for the constraints related to other objectives. However, since the spectral efficiency and energy efficiency are conflicting objectives. That is to say maximizing one objective may cause a poor performance for the others. For example, as illustrated in [16], when the system achieves the maximum energy efficiency with $M = 100$ and $T = 196$ for MRC receiver, its corresponding spectral efficiency is only 9 bits/s/Hz. Therefore, due to the diverse expectations on future wireless communication, purely maximizing one objective is no longer viable. In contrary with conventional approach, in this section, we aim at optimizing both spectral and energy efficiency for one-bit massive MIMO systems by properly allocating the resources, namely the number of active terminals K, the training length τ and the system operating power $\rho_{\rm u}$ with fixed number of BS antennas M and coherence interval T.

Before proceeding, we first define the SE and EE function by accounting both uplink and downlink. The SE is defined as the average achievable rate of the over the coherence interval T and can be given by

$$\mathcal{F}_{\rm SE} = \frac{(T-\tau)}{T}K\left(\gamma R_{\rm A}^{(\rm UL)} + (1-\gamma)R_{\rm A}^{(\rm DL)}\right), \tag{47}$$

where ${\rm A} \in \{{\rm MRC}, {\rm ZF}\}$. Accordingly, the EE is defined as average achievable rate achieved by unit transmit power, given by

$$\mathcal{F}_{\rm EE} = \frac{(T-\tau)K}{T}\frac{\gamma R_{\rm A}^{(\rm UL)} + (1-\gamma)R_{\rm A}^{(\rm DL)}}{\gamma {\rm E}\{P_{\rm total}^{(\rm UL)}\} + (1-\gamma){\rm E}\{P_{\rm total}^{(\rm DL)}\}}. \tag{48}$$

Note that the total transmit power $P_{\rm total}^{(\rm UL)}$ is changing since the active terminals are randomly selected in round-robin fashion and the large scale fading coefficients are different. Therefore, instead of considering the instantaneous total transmit power, we here consider the average total transmit power. For different channel realizations, the average total transmit power can be expressed as

$$\begin{aligned}{\rm E}\left\{P_{\rm total}^{(\rm UL)}\right\} &= \sum_{k=1}^{K} p_k = \sum_{k=1}^{K}{\rm E}\{\beta_k^{-1}\}\rho_{\rm u} \\ &= K\rho_{\rm u}\frac{r_{\rm max}^{\kappa+2} - r_{\rm min}^{\kappa+2}}{\bar{d}(1+\kappa/2)(r_{\rm max}^2 - r_{\rm min}^2)r_{\rm min}^{\kappa}}.\end{aligned} \tag{49}$$

According to the uplink-downlink duality shown in Theorem 1, any target achievable rate achieved in the uplink transmission can be achieved in the downlink while keeping the uplink and downlink transmit power unchanged with $P_{\rm total}^{(\rm UL)} = P_{\rm total}^{(\rm DL)}$, we drop the superscript of '(UL)' and '(DL)' and hence the SE and EE can be rewritten as

$$\mathcal{F}_{\rm SE} = \frac{(T-\tau)}{T}KR_{\rm A}, \tag{50}$$

$$\mathcal{F}_{\rm EE} = \frac{(T-\tau)}{T}\frac{R_{\rm A}\bar{d}(1+\kappa/2)(r_{\rm max}^2 - r_{\rm min}^2)r_{\rm min}^{\kappa}}{\rho_{\rm u}(r_{\rm max}^{\kappa+2} - r_{\rm min}^{\kappa+2})}. \tag{51}$$

Next we investigate the optimal number of users and optimal operating power that jointly maximize the spectral and energy efficiency in one-bit massive MIMO systems. The optimization problem can be mathematically formulated as

$$(K^\star, \tau^\star, \rho^\star) = \arg\max_{K,\tau,\rho} \quad \{\mathcal{F}_{\rm SE}, \mathcal{F}_{\rm EE}\}. \tag{52}$$

Obviously the optimization problem has two objective functions, which is known as multiple objective optimization (MOO) or vector optimization problem. In contrast to single-objective optimization, a single global solution to a multiple objective optimization problem that maximizes both spectral efficiency and energy efficiency usually does not exist. In fact, the operating point that simultaneously maximizing both spectral and energy efficiency is defined as the utopia point $\mathbf{f}_{\rm utopia}$, yields,

$$\mathbf{f}_{\rm utopia} = [\mathcal{F}_{\rm SE}^{\rm max}, \mathcal{F}_{\rm EE}^{\rm max}]^T = \begin{bmatrix} \max\limits_{K,\tau,\rho} & \mathcal{F}_{\rm SE} \\ \max\limits_{K,\tau,\rho} & \mathcal{F}_{\rm EE} \end{bmatrix}. \tag{53}$$

Then a natural question is what kind of solutions we should pursue when investigating the MOO problem. Therefore, the Pareto boundary is introduced, which has the property that none of the objectives can be improved without degrading other objectives. The Pareto optimal point is then defined as the point that can be mapped to the Pareto boundary.

There are two methods to solve the MOO problem: the a posterior method and the a priori method. For the a posterior method, the system needs to know the Pareto boundary and make an informed decision to select a specific solution under

the system subjective preference. One approach to obtain the Pareto boundary is known as the weighted Chebyshev problem, whose main idea is to search for the outermost point in different directions and can be expressed as:

$$\begin{aligned} &\text{maximize} \quad \lambda \\ &\text{subject to} \quad \mathcal{F}_{\text{ob}} \geq \lambda v_{\text{ob}}, \quad \text{ob} \in \{\text{SE}, \text{EE}\} \end{aligned} \tag{54}$$

where the weights of v_{SE} and v_{EE} can be regarded as the search direction for spectral and energy efficiency, respectively. To guarantee the resolution of the Pareto optimal operation solutions, the system may need to search all the directions, which may lead to high complexity. Therefore, in order to avoid this drawback, we mainly focus on the a priori method in the following.

A. The a Priori Method

The a priori method allows the system to specify preferences, which may be articulated in terms of goals or the relative importance of different objectives, and then the system finds the operating point that satisfies these preferences as well as possible. In particular, the multi objective optimization problem with high complexity is reformulated into a single objective optimization problem. One of the most common methods is the weighted sum method to reformulate (52) as:

$$(K^\star, \tau^\star, \rho^\star) = \arg \max_{K,\tau,\rho} \quad (w_{\text{SE}}\mathcal{F}_{\text{SE}} + w_{\text{EE}}\mathcal{F}_{\text{EE}}), \tag{55}$$

where the weights w_{SE} and w_{EE} reflect the relative importance of the objectives. Note that, by using the weighted sum methods, a constraints of $w_{\text{SE}} + w_{\text{EE}} = 1$ is often assumed [21]. However, it has been stated in [18] that if all of the weight are positive, then the maximum of this problem is Pareto optimal. Therefore, we assume that there is no constraint of the weights w_{SE} and w_{EE} in (55).

However, when the objective function in (55) is non-convex (especially the concave case), the solution in (55) may result in poor performance. As we will see in the numerical results of Fig. 4, the solution of the sum weighted method is almost overlapped to the solution of maximizing EE problem, both of which lead to a poor performance of SE. To avoid this, we next introduce the weighted product method, which can be expressed as

$$(K^\star, \tau^\star, \rho_{\text{u}}^\star) = \arg \max_{K,\tau,\rho} \quad (\mathcal{F}_{\text{SE}})^{w_{\text{SE}}} \cdot (\mathcal{F}_{\text{EE}})^{w_{\text{EE}}}, \tag{56}$$

where the weights w_{SE} and w_{EE} indicating the relative significance of the objective functions. Note that (55) is the weighted arithmetic mean while (56) is the weighted geometric mean. The advantages of the weighted product method are: i) it allows the objective functions with different scales to have similar significance; ii) it can avoid having to transform objective functions since the relative scaling has no impact. A specific Pareto optimal operating point that is provided as the solution depends on which weights are used. For example, if $w_{\text{SE}} \neq 0$ and $w_{\text{EE}} = 0$, then the optimization problem reduce to maximize the spectral efficiency only, which indicates that the system is only interested in the spectral efficiency performance and ignore the energy efficiency. And vice versa if $w_{\text{SE}} = 0$ and $w_{\text{EE}} \neq 0$. Thus it is important to determine the weights w_{SE} and w_{EE}. Since both spectral and energy efficiency are important in future wireless communication systems, we can define the weights of w_{SE} and w_{EE} as the 'importance' of each objective function. Therefore, if both spectral and energy efficiency have equal importance, we can select the weights $w_{\text{SE}} = w_{\text{EE}} = 1$.

Note that, by using the uplink-downlink duality, it is guaranteed that the set of optimal solutions for the number of active terminals $K^\star$, training length $\tau^\star$ and the operating power $\rho_{\text{u}}^\star$ is optimal for both uplink and downlink.

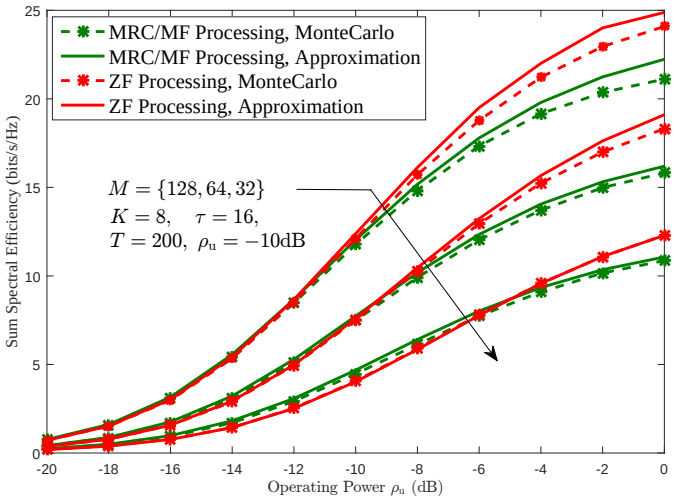

Fig. 2. Sum spectral efficiency versus operating power ρ_{u} with $M = \{32, 64, 128\}$, $K = 8$, $T = 200$ and $\tau = 16$ for MRC/MF and ZF processing.

VII. Numerical Results

For our simulations, we consider a cell with a radius of 500 meters and all $K_{\max}$ terminals distributed randomly and uniformly over the cell, with the exclusion of a central disk of radius 100 meter. According to the [36], we choose $\bar{d} = 10^{0.8}$ and $\kappa = 3.8$ for a typical urban cellular environment.

We first evaluate the validity of the approximations on the achievable rate for the MRC and ZF receivers derived in Theorems 2 and 3 compared with the ergodic rate given in (33). Fig. 2 shows the sum spectral efficiency versus operating power ρ_{u} for different numbers of transmit antennas $M = \{32, 64, 128\}$. We also choose the length of the coherence interval to be $T = 200$, the number of active terminals $K = 8$, and training length $\tau = 16$, such that the relative pilot length $\tau_0 = 2$. The straight lines represent the sum spectral efficiencies obtained numerically from (42) and (43), respectively, while the dash lines with marker represent the ergodic sum spectral efficiencies obtained from (33). Apparently, for both the MRC and ZF processing, the gap between the bounds and the empirical ergodic rates is small, especially in the low operating power region. This implies that the approximation on the achievable rate given in (42) and (43) is a good predictor of the performance of one-bit massive MIMO systems. Thus, in the following plots we will show only the approximation when evaluating performance.

In the downlink, as analyzed in previous sections, since each transmit antenna should equip with a power amplifier in order

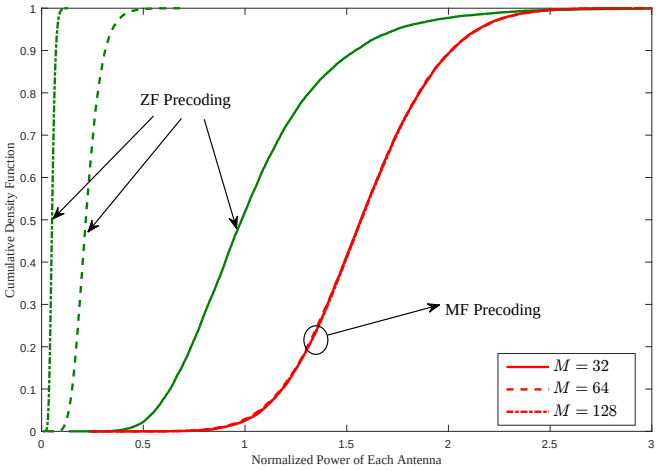

Fig. 3. Cumulative density function of the normalized downlink transmission power of each antenna over 500 channel realizations with different numbers of transmit antennas M and $\rho_{\rm u} = -10$dB.

to implement the power allocation in (31), it is necessary that the power amplifier should work in a relative small dynamic range. Fig. 3 shows the cumulative density function of the normalized downlink transmission power of each antenna with $M = \{32, 64, 128\}$ and operating power $\rho_{\rm u} = -10$dB for MF and ZF precoding in (44) and (45), respectively. The power allocation matrix follows the scheme in (46) and the power of each transmit antenna is normalized by the operating power $\rho_{\rm u}$. We can easily see that the dynamic ranges of the power amplifier are indeed small. We interestingly note that for different number of transmit antennas, the dynamic range for the MF precoding stays the same, while the dynamic range for ZF precoding decreases with the increase of the number of transmit antennas. In addition, according to the uplink-downlink duality and Fig. 2, when the MF and ZF precoding achieve almost the same rate at $\rho_{\rm u} = -10$dB, the normalized transmission power for ZF precoding is smaller than the MF precoding. This implies that, in order to achieve the same rate in downlink transmission, the ZF precoding can use less power than the MF precoding.

Next we describe how the multiple objective optimization problem can be used to study tradeoffs between the spectral and energy efficiency. In conventional massive MIMO systems, a common rule of thumb is that the number of BS antennas M should be 10 times more than the number of active terminals K and the optimal pilot training length should be equal to the number of active terminals, such that $\tau = K$. An interesting questions is whether the aforementioned rule is still true in one-bit massive MIMO systems? To answer this question, Fig.3 illustrates the energy efficiency versus its corresponding spectral efficiency with different number of BS antennas M and coherence interval $T = 400$ for MRC/MF and ZF processing, respectively. The solid lines and the dash-dot line represents the Pareto boundary of optimal design and unquantized case [16], respectively, where the number of active terminals K, the training length τ and the operating power $\rho_{\rm u}$ are jointly optimized. The dash line represents the Pareto boundary of the benchmark case, which are obtained by setting $K = 0.1M$, $\tau = K$ and only optimizing the operating power $\rho_{\rm u}$.

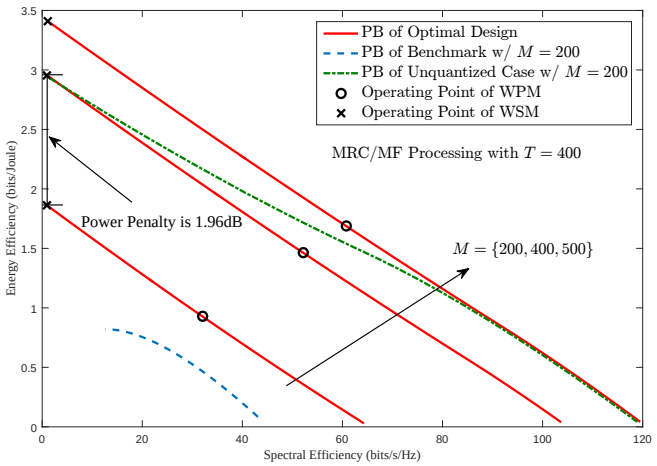
PB of Optimal Design
PB of Benchmark w/ $M = 200$
PB of Unquantized Case w/ $M = 200$
Operating Point of WPM
Operating Point of WSM
MRC/MF Processing with $T = 400$
Power Penalty is 1.96dB
$M = \{200, 400, 500\}$
Energy Efficiency (bits/Joule)
Spectral Efficiency (bits/s/Hz)

(a)

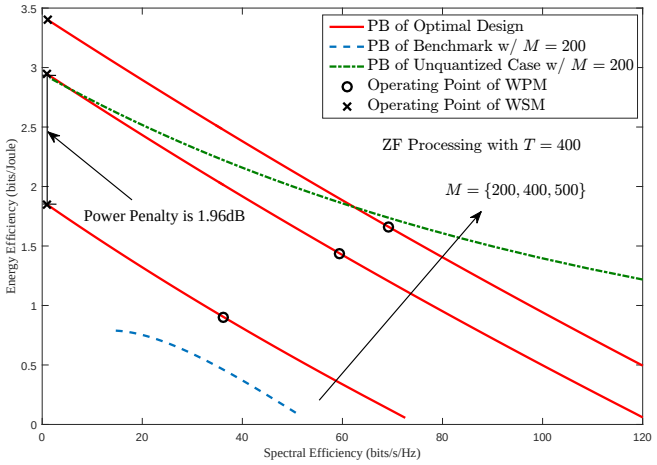
PB of Optimal Design
PB of Benchmark w/ $M = 200$
PB of Unquantized Case w/ $M = 200$
Operating Point of WPM
Operating Point of WSM
ZF Processing with $T = 400$
Power Penalty is 1.96dB
$M = \{200, 400, 500\}$
Energy Efficiency (bits/Joule)
Spectral Efficiency (bits/s/Hz)

(b)

Fig. 4. Pareto boundary of energy efficiency versus spectral efficiency for optimal design, benchmark and unquantized case with $M = \{200, 400, 500\}$ and $T = 400$ for (a) MRC/MF processing and (b) ZF processing.

First, by looking at the Pareto boundary of the optimal design, we can see that when the energy efficiency is maximized, its corresponding spectral efficiency is extreme low. For example, for MRC/MF processing with $M = 200$, when the energy efficiency achieve its maximum value, the spectral efficiency is only 0.88 bits/s/Hz, which is far from being expected in future wireless network. Moreover, a very marked conflicting between the spectral and energy efficiency can be observed since the spectral efficiency can only be improved by making drastic sacrifices in energy efficiency. We note that the energy efficiency is almost a linear function with respect to the spectral efficiency. This implies that, for instance, if we want to make an improvement of 10% in spectral efficiency, the energy efficiency will be sacrificed by almost 10%.

Then, comparing the Pareto boundary of the optimal design with the benchmark case, we see that for each operating point of the 'Benchmark' curve, we can always find an operating point with higher spectral and energy efficiency on the 'Optimal Design' curve, since the 'Benchmark' curve lies inside of the optimal one.

We next compare the Pareto boundary of the optimal design

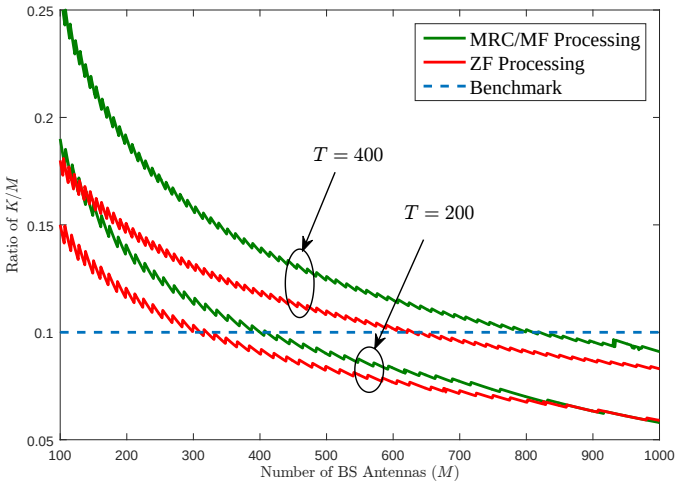

Fig. 5. Ratio of K/M versus the number of BS antennas M with different coherence interval T for MRC/MF and ZF processing.

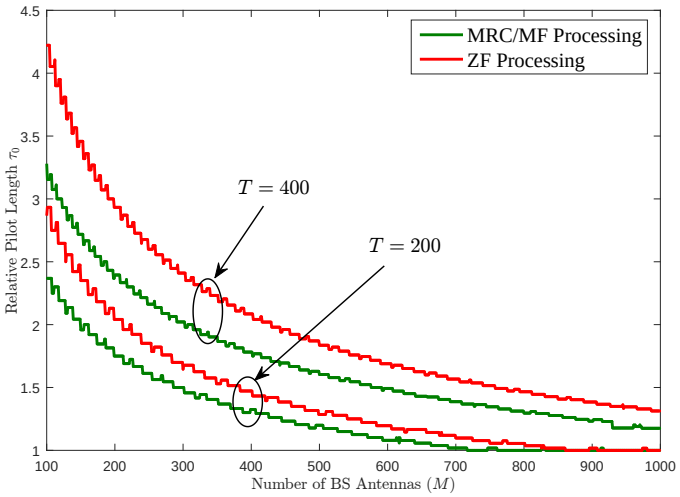

Fig. 6. Optimal relative pilot length τ_0 versus the number of BS antennas M with different coherence interval T for MRC/MF and ZF processing.

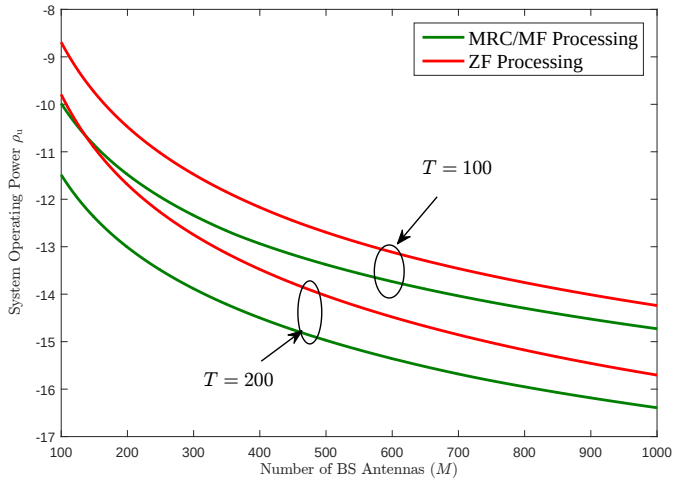

Fig. 7. Optimal system operating power ρ_{u} versus the number of BS antennas M with different coherence interval T for MRC/MF and ZF processing.

with the unquantized case. We see that when the spectral efficiency of both cases are extremely low (and hence the system operating power is also extremely low), the power penalty of one-bit systems observed in [11] can be verified. In addition, it is interesting to note that, the power penalty of one-bit massive MIMO system can be compensated by deploying 2 times more antennas at the BS in the low system operating power region for both MRC/MF and ZF processings. With increasing spectral efficiency (and hence, the system operating power increases), the power penalty of one-bit system can be compensated by deploying at most 2.5 times more antennas for MRC/MF processing, while for ZF processing, however, an ever increasing number of antennas in the one-bit system would be needed to compensate the power penalty. This is because, with increasing power, the ZF processing in unquantized case is theoretically able to obtain a better channel estimation that allows it to significantly eliminate all inter-user interference, while in one-bit case, it cannot.

The points with cross marker and circle marker in Fig.4 represents the system operating point obtained by the weighted sum method and the weighted product method, respectively. The weights w_{SE} and w_{EE} are chosen by utilizing the utopia point $[w_{\mathrm{SE}}^{-1}, w_{\mathrm{EE}}^{-1}] = \mathbf{f}_{\mathrm{utopia}}^{T}$ for weighted sum method, while $[w_{\mathrm{SE}}, w_{\mathrm{EE}}] = [1, 1]$ for weighted product method for attaining equal importance of both spectral and energy efficiency. Clearly, the weighted sum method will achieve at the maximum-energy-efficiency operating point, while the weighted product method can achieve a compromised operating point with reasonable spectral and energy efficiency. This is because the objective function in (52) is neither convex nor concave and the weighted sum method is unable to capture points on non-convex portions of the Pareto boundary. Therefore, we only employ the weighted product method to solve the multiple objective optimization problem of (52) in the following.

Fig.5-6 show the ratio of $K^{\star}/M$ and relative training length τ_0 versus the number of BS antennas M with different coherence interval T. We can see from the plots that the optimal number of active terminals and pilot training length might not following the assumption of $K = 0.1M$ and $\tau = K$. Generally, for practical massive MIMO deployment with $M \leq 500$, more terminals should be activated in one-bit systems rather than following the conventional assumption of $K = 0.1M$. In addition, we observe that more relative pilot length is necessary to combat the quantization noise in one-bit systems.

Since all our analysis results are obtained on basis of the low operating power assumption, we finally verify that whether this assumption is reasonable or not. Fig. 7 illustrated the operating power ρ_{u} versus the number of BS antennas M for MRC/MF and ZF processing with different coherence interval. As we can see from the plot, for both linear processings, the system operating power region is below -10 dB in general, which implies that our low operating power assumption is justified, especially the coherence interval and the number of BS antennas are both large. In addition, combining Fig. 5 with Fig. 7, it is interesting to note that the MRC/MF processing is more competitive than the ZF processing since it can utilize less power while serve more terminals with lower computational complexity.

VIII. Conclusions

This paper has investigated the optimal design for single-cell massive MIMO system when one-bit ADC/DACs equipped at the BS. We first provided the statistically equivalent linear signal model for one-bit quantization by using Bussgang decomposition. Then we derived approximate closed-form expressions at low system operating power for uplink achievable rate assuming MRC and ZF receivers that employ the imperfect CSI. In fact, with our proposed precoding schemes and downlink power allocation, the approximate expressions are the same for uplink and downlink. This duality property allows us to optimize the performance of the network by considering uplink and downlink transmission simultaneously. Since EE and SE are conflicting objectives, we then used the multiple objective optimization framework to investigate the EE-SE tradeoff issues for the one-bit massive MIMO. The Pareto boundary of the EE versus SE can be obtained by a posterior method and allows the system to balance the EE and SE in an efficient way. In order to reduce the computational complexity of the a posterior method, the a priori method such as the weighted product method is used to optimized EE and SE with equal importance. Numerical results illustrated the fundamental tradeoff between EE and SE in one-bit quantization systems for different system parameter settings and showed that the EE is almost a linear function with respect to SE. Comparing with the unquantized case, we showed that the power penalty in one-bit system can be compensated by deploying 2-2.5 times more antennas at BS, while significantly more antennas are required in a one-bit system for the ZF processing. In addition, we showed that, with the weighted product method where both SE and EE are optimized with equal importance, the optimal number of active terminals, the training length does not follow the common assumption in conventional massive MIMO systems.

Appendix A

Suppose γ_k is the target SINR achieved by the kth active user for both uplink and downlink transmission. For the downlink transmission, we assume the precoding vector yields:

$$\mathbf{t}_k = \sqrt{q_k}\hat{\mathbf{t}}_k. \tag{57}$$

where $q_k = \|\mathbf{t}_k\|_2^2$, $\hat{\mathbf{t}}_k = \mathbf{t}_k/q_k$ with $\|\hat{\mathbf{t}}_k\|_2^2 = 1$, and the power allocation for the downlink transmission yields:

$$\mathbf{Q} = \sqrt{\frac{\pi}{2}}\text{diag}\left(\sum_{i=1}^{K}\mathbf{t}_i\mathbf{t}_i^H\right)^{\frac{1}{2}}. \tag{58}$$

With these two notation, we have

$$P_{\text{total}}^{(\text{DL})} = \text{tr}(\mathbf{Q}\mathbf{Q}^H) = \frac{\pi}{2}\sum_{i=1}^{K} q_i \tag{59}$$

which allows us to transfer the problem of power allocation of each antenna into the problem of power allocation of each precoding vector. Substituting it into (24), the downlink SINR can be expressed as

$$\gamma_k = \frac{q_k|\mathbf{g}_k^T\hat{\mathbf{t}}_k|^2}{\sum_{i\neq k}^{K} q_i|\mathbf{g}_k^T\hat{\mathbf{t}}_i|^2 + (\frac{\pi}{2}-1)\mathbf{g}_k^T\text{diag}(\sum_{i=1}^{K} q_i\hat{\mathbf{t}}_i\hat{\mathbf{t}}_i^H)\mathbf{g}_k^* + 1}. \tag{60}$$

Then we define a $K\times K$ matrix $\mathbf{\Psi}$, whose (k,i)th element is given by

$$[\mathbf{\Psi}]_{k,i} = \begin{cases} |\mathbf{g}_k^T\hat{\mathbf{t}}_i|^2 + \left(\frac{\pi}{2}-1\right)\mathbf{g}_k^T\text{diag}\left(\hat{\mathbf{t}}_i\hat{\mathbf{t}}_i^H\right)\mathbf{g}_k^*, & i\neq k \\ \left(\frac{\pi}{2}-1\right)\mathbf{g}_k^T\text{diag}\left(\hat{\mathbf{t}}_i\hat{\mathbf{t}}_i^H\right)\mathbf{g}_k^*, & i = k \end{cases} \tag{61}$$

Moreover, we define the $K\times K$ diagonal matrix $\mathbf{D}$, whose kth diagonal entry is given by

$$[\mathbf{D}]_{k,k} = \gamma_k\left|\mathbf{g}_k^T\hat{\mathbf{t}}_k\right|^{-2}. \tag{62}$$

Using this notation, (60) can be rewrite as

$$[\mathbf{D}]_{k,k} = \frac{q_k}{\sum_{i=1}^{K} q_i[\mathbf{\Psi}]_{k,i} + 1}. \tag{63}$$

Therefore, according to (68) we can express the downlink SINR conditions for all active users as

$$\mathbf{q} = \mathbf{D}\mathbf{\Psi}\mathbf{q} + \mathbf{D}\mathbf{1}_K \Leftrightarrow \mathbf{q} = (\mathbf{I}-\mathbf{D}\mathbf{\Psi})^{-1}\mathbf{D}\mathbf{1}_K, \tag{64}$$

where $\mathbf{q} = [q_1,...,q_k]^T$ and $\mathbf{1}_K$ denotes all-one vector.

For the uplink transmission, we assume that $\mathbf{w}_k^T\mathbf{A}_u = \mathbf{t}_k^T = \sqrt{q_k}\hat{\mathbf{t}}_k^T$ and substituting it into (23), yields:

$$\gamma_k = \frac{p_k|\hat{\mathbf{t}}_k^T\mathbf{g}_k|^2}{\sum_{i\neq k}^{K} p_i|\hat{\mathbf{t}}_k^T\mathbf{g}_i|^2 + \|\hat{\mathbf{t}}_k^T\|_2^2 + \omega\hat{\mathbf{t}}_k^T\mathbf{A}_u^{-2}\hat{\mathbf{t}}_k}. \tag{65}$$

After substituting (17) into (65) and $\|\hat{\mathbf{t}}_k^T\|_2^2 = 1$, the denominator of (65) can be expressed as

$$\begin{aligned} &\sum_{i\neq k}^{K} p_i|\hat{\mathbf{t}}_k^T\mathbf{g}_i|^2 + 1 + \left(\frac{\pi}{2}-1\right)\hat{\mathbf{t}}_k^T\text{diag}\left(\sum_{i=1}^{K} p_i\mathbf{g}_i\mathbf{g}_i^H + \mathbf{I}\right)\hat{\mathbf{t}}_k \\ &= \sum_{i\neq k}^{K} p_i|\hat{\mathbf{t}}_k^T\mathbf{g}_i|^2 + \left(\frac{\pi}{2}-1\right)\hat{\mathbf{t}}_k^T\text{diag}\left(\sum_{i=1}^{K} p_i\mathbf{g}_i\mathbf{g}_i^H\right)\hat{\mathbf{t}}_k + \frac{\pi}{2} \\ &= \sum_{i\neq k}^{K} p_i|\hat{\mathbf{t}}_k^T\mathbf{g}_i|^2 + \left(\frac{\pi}{2}-1\right)\sum_{i=1}^{K} p_i\mathbf{g}_i^T\text{diag}\left(\hat{\mathbf{t}}_k\hat{\mathbf{t}}_k^H\right)\mathbf{g}_i + \frac{\pi}{2}. \end{aligned} \tag{66}$$

The third line of (66) holds thanks to the following identity for two matrices $\mathbf{A}$, $\mathbf{B}$:

$$\text{tr}(\mathbf{A}\text{diag}(\mathbf{B})) = \text{tr}(\mathbf{B}\text{diag}(\mathbf{A})). \tag{67}$$

By using the notation of (61) and (62), we can then express (65) as

$$[\mathbf{D}]_{k,k} = \frac{p_k}{\sum_{i=1}^{K} p_i[\mathbf{\Psi}]_{i,k} + \frac{\pi}{2}}. \tag{68}$$

After stacking it into vector form, we have

$$\mathbf{p} = \mathbf{D}\mathbf{\Psi}^T\mathbf{p} + \frac{\pi}{2}\mathbf{D}\mathbf{1}_K \Leftrightarrow \mathbf{p} = \frac{\pi}{2}(\mathbf{I}-\mathbf{D}\mathbf{\Psi}^T)^{-1}\mathbf{D}\mathbf{1}_K, \tag{69}$$

where $\mathbf{p} = [p_1,...,p_K]^T$. Since the eigenvalue of $(\mathbf{I}-\mathbf{D}\mathbf{\Psi})$ and $(\mathbf{I}-\mathbf{D}\mathbf{\Psi}^T)$ are the same, therefore we can verify the total

transmit power for the uplink and downlink are the same:

$$P_{\text{total}}^{(\text{UL})} = \|\mathbf{p}\|_1 = \frac{\pi}{2}\|\mathbf{q}\|_1 = P_{\text{total}}^{(\text{DL})}. \tag{70}$$

Thus we complete the proof.

APPENDIX B

From (38), we first focus on deriving the terms of $\mathrm{E}\left\{\left|\mathbf{w}_k^T\mathbf{g}_k^{\text{eff}}\right|^2\right\}$, $\mathrm{E}\left\{\left|\mathbf{w}_k^T\mathbf{g}_i^{\text{eff}}\right|^2\right\}$. For MRC receiver, we have

$$\mathbf{w}_k^T\mathbf{g}_k^{\text{eff}} = (\hat{\mathbf{g}}_k^{\text{eff}})^H\hat{\mathbf{g}}_k^{\text{eff}} + (\hat{\mathbf{g}}_k^{\text{eff}})^H\boldsymbol{\varepsilon}_k. \tag{71}$$

Since the elements of the estimated effective channel $(\hat{\mathbf{g}}_k^{\text{eff}})$ are i.i.d, according to [37] we can thus obtain

$$\begin{aligned}\mathrm{E}\left\{\left|\mathbf{w}_k^T\mathbf{g}_k^{\text{eff}}\right|^2\right\} &= \mathrm{E}\left\{\left|(\hat{\mathbf{g}}_k^{\text{eff}})^H\hat{\mathbf{g}}_k^{\text{eff}}\right|^2\right\} + \mathrm{E}\left\{\left|(\hat{\mathbf{g}}_k^{\text{eff}})^H\boldsymbol{\varepsilon}_k\right|^2\right\} \\ &= \sigma^4(M^2+M) + \sigma^2(\rho_{\text{u}}-\sigma^2)M = \sigma^2M(\sigma^2M+\rho_{\text{u}}).\end{aligned} \tag{72}$$

For $i \neq k$, we have

$$\mathrm{E}\left\{\left|(\hat{\mathbf{g}}_k^{\text{eff}})^H\mathbf{g}_i^{\text{eff}}\right|^2\right\} = \mathrm{Var}\left\{(\hat{\mathbf{g}}_k^{\text{eff}})^H\mathbf{g}_i^{\text{eff}}\right\} = \rho_{\text{u}}\sigma^2M. \tag{73}$$

Then we focus on deriving the term of AQN_k. Since the expectation is taken with respect to the channel realizations. For different channel realizations, the covariance matrix of the quantization noise $\boldsymbol{\eta}_u$ is given by

$$\mathrm{E}\{\boldsymbol{\eta}_{\text{u}}\boldsymbol{\eta}_{\text{u}}^H\} = \mathrm{E}\{\mathbf{r}_{\text{u}}\mathbf{r}_{\text{u}}^H\} - \alpha_{\text{u}}^2\mathrm{E}\{\mathbf{y}_{\text{u}}\mathbf{y}_{\text{u}}^H\} = (1-2/\pi)\mathbf{I}. \tag{74}$$

By using the Bussgang decomposition, $\boldsymbol{\eta}_{\text{u}}$ is not only uncorrelated with the received signal $\mathbf{y}_{\text{u}}$, but it is also uncorrelated with the effective channel $\mathbf{g}_k^{\text{eff}}$. We rewrite AQN_k as

$$\mathrm{AQN}_k = (\alpha_{\text{u}}^2 + 1 - 2/\pi)\mathrm{E}\left\{\left\|\mathbf{w}_k^T\right\|_2^2\right\}. \tag{75}$$

With MRC receiver $\mathbf{w}_k^T = (\hat{\mathbf{g}}_k^{\text{eff}})^H$, we have

$$\mathrm{AQN}_k = (\alpha_{\text{u}}^2 + 1 - 2/\pi)\sigma^2M. \tag{76}$$

Substituting (72)-(76) into (38), we can arrive at Theorem 2.

APPENDIX C

For the ZF receiver, we have

$$\mathbf{W}_{\text{ZF}}^T\mathbf{G}_{\text{eff}} = \mathbf{W}_{\text{ZF}}^T(\hat{\mathbf{G}}_{\text{eff}} + \mathcal{E}_{\text{eff}}) = \mathbf{I} + \mathbf{W}_{\text{ZF}}^T\mathcal{E}_{\text{eff}}, \tag{77}$$

where $\mathcal{E}_{\text{eff}} = [\boldsymbol{\varepsilon}_1^{\text{eff}}, ..., \boldsymbol{\varepsilon}_K^{\text{eff}}]$. Therefore we have

$$\mathbf{w}_k^T\mathbf{g}_k^{\text{eff}} = 1 + \mathbf{w}_k^T\boldsymbol{\varepsilon}_k^{\text{eff}}, \tag{78}$$

and $\mathrm{E}\left\{\left|\mathbf{w}_k^T\mathbf{g}_k^{\text{eff}}\right|^2\right\}$ can be expressed as

$$\begin{aligned}\mathrm{E}\left\{\left|\mathbf{w}_k^T\mathbf{g}_k^{\text{eff}}\right|^2\right\} &= 1 + \mathrm{E}\{|\mathbf{w}_k^T\boldsymbol{\varepsilon}_k^{\text{eff}}|^2\} \\ &= 1 + (\rho_{\text{u}}-\sigma^2)\mathrm{E}\left\{\left[\left(\hat{\mathbf{G}}_{\text{eff}}^H\hat{\mathbf{G}}_{\text{eff}}\right)^{-1}\right]_{k,k}\right\}.\end{aligned} \tag{79}$$

Since the elements of $\hat{\mathbf{G}}^{\text{eff}}$ are approximated as i.i.d Gaussian distribute, $\left(\hat{\mathbf{G}}^{\text{eff}}\right)^H\hat{\mathbf{G}}^{\text{eff}}$ is a $K \times K$ central Wishart matrix with M degrees of freedom. Thus

$$\mathrm{E}\left\{\left|\mathbf{w}_k^T\mathbf{g}_k^{\text{eff}}\right|^2\right\} = 1 + \frac{\rho_{\text{u}}-\sigma^2}{\sigma^2(M-K)}. \tag{80}$$

For $i \neq k$, we have

$$\begin{aligned}\mathbf{w}_k^T\mathbf{g}_i^{\text{eff}} &= \mathrm{E}\{|\mathbf{w}_k^T\boldsymbol{\varepsilon}_i^{\text{eff}}|^2\} \\ &= (\rho_{\text{u}}-\sigma^2)\mathrm{E}\left\{\left[\left(\hat{\mathbf{G}}_{\text{eff}}^H\hat{\mathbf{G}}_{\text{eff}}\right)^{-1}\right]_{k,k}\right\} \\ &= \frac{\rho_{\text{u}}-\sigma^2}{\sigma^2(M-K)}.\end{aligned} \tag{81}$$

Similarly, we can obtain

$$\mathrm{AQN}_k = \frac{\alpha_{\text{u}}^2 + 1 - 2/\pi}{\zeta_k^2(M-K)}. \tag{82}$$

Substituting (79)-(82) into (38), we can arrive at Theorem 3.

REFERENCES

[1] T. Marzetta, "Noncooperative cellular wireless with unlimited numbers of base station antennas," *IEEE Transactions on Wireless Communications*, vol. 9, no. 11, pp. 3590–3600, November 2010.

[2] L. Lu, G. Y. Li, A. L. Swindlehurst, A. Ashikhmin, and R. Zhang, "An overview of massive MIMO: Benefits and challenges," *IEEE Journal of Selected Topics in Signal Processing*, vol. 8, no. 5, pp. 742–758, 2014.

[3] E. Larsson, O. Edfors, F. Tufvesson, and T. Marzetta, "Massive MIMO for next generation wireless systems," *IEEE Communications Magazine*, vol. 52, no. 2, pp. 186–195, February 2014.

[4] F. Rusek, D. Persson, B. K. Lau, E. Larsson, T. Marzetta, O. Edfors, and F. Tufvesson, "Scaling up MIMO: Opportunities and challenges with very large arrays," *IEEE Signal Processing Magazine*, vol. 30, no. 1, pp. 40–60, Jan 2013.

[5] "Texas instruments ADC products." [Online]. Available: http://www.ti.com/lsds/ti/data-converters/analog-to-digital-converter-products.page

[6] C. Risi, D. Persson, and E. G. Larsson, "Massive MIMO with 1-bit ADC." [Online]. Available: http://arxiv.org/abs/1404.7736

[7] J. Choi, J. Mo, and R. Heath, "Near maximum-likelihood detector and channel estimator for uplink multiuser massive MIMO systems with one-bit ADCs." [Online]. Available: http://arxiv.org/abs/1507.04452

[8] Y. Li, C. Tao, L. Liu, A. Mezghani, G. Seco-Granados, and A. Swindlehurst, "Channel estimation and uplink achievable rate in one-bit massive MIMO systems," *submitted to IEEE Transactions on Signal Processing*.

[9] C. Mollén, J. Choi, E. G. Larsson, and R. W. H. Jr., "Performance of the wideband massive uplink MIMO with one-bit ADCs." [Online]. Available: https://arxiv.org/abs/1602.07364

[10] A. Mezghani and J. Nossek, "Analysis of Rayleigh-fading channels with 1-bit quantized output," in *IEEE International Symposium on Information Theory (ISIT)*, July 2008, pp. 260–264.

[11] J. A. Nossek and M. T. Ivrlač, "Capacity and coding for quantized MIMO systems," in *Proceedings of the international conference on Wireless communications and mobile computing*. ACM, 2006, pp. 1387–1392.

[12] E. Bjornson, E. G. Larsson, and M. Debbah, "Massive MIMO for maximal spectral efficiency: How many users and pilots should be allocated?" *IEEE Transactions on Wireless Communications*, vol. 15, no. 2, pp. 1293–1308, Feb 2016.

[13] H. Q. Ngo, M. Matthaiou, and E. G. Larsson, "Massive MIMO with optimal power and training duration allocation," *IEEE Wireless Communications Letters*, vol. 3, no. 6, pp. 605–608, Dec 2014.

[14] C. Han, T. Harrold, S. Armour, I. Krikidis, S. Videv, P. M. Grant, H. Haas, J. S. Thompson, I. Ku, C. X. Wang, T. A. Le, M. R. Nakhai, J. Zhang, and L. Hanzo, "Green radio: radio techniques to enable energy-efficient wireless networks," *IEEE Communications Magazine*, vol. 49, no. 6, pp. 46–54, June 2011.

[15] Y. Chen, S. Zhang, S. Xu, and G. Y. Li, "Fundamental trade-offs on green wireless networks," *IEEE Communications Magazine*, vol. 49, no. 6, pp. 30–37, June 2011.

[16] H. Q. Ngo, E. Larsson, and T. Marzetta, "Energy and spectral efficiency of very large multiuser MIMO systems," *IEEE Transactions on Communications*, vol. 61, no. 4, pp. 1436–1449, April 2013.

[17] E. Bjornson, L. Sanguinetti, J. Hoydis, and M. Debbah, "Optimal design of energy-efficient multi-user MIMO systems: Is massive MIMO the answer?" *IEEE Transactions on Wireless Communications*, vol. 14, no. 6, pp. 3059–3075, June 2015.

[18] R. T. Marler and J. S. Arora, "Survey of multi-objective optimization methods for engineering," *Structural and multidisciplinary optimization*, vol. 26, no. 6, pp. 369–395, 2004.

[19] J. Branke, K. Deb, K. Miettinen, and R. Slowiński, *Multiobjective optimization: interactive and evolutionary approaches*. Springer, 2008, vol. 5252.

[20] E. Bjornson, E. A. Jorswieck, M. Debbah, and B. Ottersten, "Multiobjective signal processing optimization: The way to balance conflicting metrics in 5G systems," *IEEE Signal Processing Magazine*, vol. 31, no. 6, pp. 14–23, 2014.

[21] J. Tang, D. K. C. So, E. Alsusa, and K. A. Hamdi, "Resource efficiency: A new paradigm on energy efficiency and spectral efficiency tradeoff," *IEEE Transactions on Wireless Communications*, vol. 13, no. 8, pp. 4656–4669, Aug 2014.

[22] C. He, B. Sheng, P. Zhu, X. You, and G. Y. Li, "Energy- and spectral-efficiency tradeoff for distributed antenna systems with proportional fairness," *IEEE Journal on Selected Areas in Communications*, vol. 31, no. 5, pp. 894–902, May 2013.

[23] Z. Zhang, Z. Chen, M. Shen, and B. Xia, "Spectral and energy efficiency of multipair two-way full-duplex relay systems with massive MIMO," *IEEE Journal on Selected Areas in Communications*, vol. 34, no. 4, pp. 848–863, April 2016.

[24] Y. Hao, Z. Song, S. Hou, and H. Li, "Energy- and spectral-efficiency tradeoff in massive MIMO systems with inter-user interference," in *IEEE 26th Annual International Symposium on Personal, Indoor, and Mobile Radio Communications (PIMRC)*, Aug 2015, pp. 553–557.

[25] L. Liu, D. W. Matolak, C. Tao, Y. Li, B. Ai, and H. Chen, "Channel capacity investigation of a linear massive MIMO system using spherical wave model in los scenarios," *Science China Information Sciences*, vol. 59, no. 2, pp. 1 – 15, 2016.

[26] J. J. Bussgang, "Crosscorrelation functions of amplitude-distorted Gaussian signals," MIT Research Lab. Electronics, Tech. Rep. 216, 1952.

[27] M. Biguesh and A. B. Gershman, "Downlink channel estimation in cellular systems with antenna arrays at base stations using channel probing with feedback," *EURASIP Journal on Applied Signal Processing*, vol. 2004, pp. 1330–1339, 2004.

[28] O. Bar-Shalom and A. Weiss, "DOA estimation using one-bit quantized measurements," *IEEE Transactions on Aerospace and Electronic Systems*, vol. 38, no. 3, pp. 868–884, 2002.

[29] S. M. Kay, *Fundamentals of statistical signal processing: Estimation Theory*. Upper Saddle River, NJ, USA: Prentice Hall, 1993.

[30] G. Jacovitti and A. Neri, "Estimation of the autocorrelation function of complex Gaussian stationary processes by amplitude clipped signals," *IEEE Transactions on Information Theory*, vol. 40, no. 1, pp. 239–245, Jan 1994.

[31] Y. Zhang and B. Yu, "The inverse of circulant matrix," *J. Math*, vol. 5, pp. 29–31, 1989.

[32] S. Vishwanath, N. Jindal, and A. Goldsmith, "Duality, achievable rates, and sum-rate capacity of Gaussian MIMO broadcast channels," *IEEE Transactions on Information Theory*, vol. 49, no. 10, pp. 2658–2668, 2003.

[33] B. Hassibi and B. Hochwald, "How much training is needed in multiple-antenna wireless links?" *IEEE Transactions on Information Theory*, vol. 49, no. 4, pp. 951–963, April 2003.

[34] H. Cramér, *Random variables and probability distributions*. Cambridge University Press, 2004, vol. 36.

[35] Q. Zhang, S. Jin, K.-K. Wong, H. Zhu, and M. Matthaiou, "Power scaling of uplink massive MIMO systems with arbitrary-rank channel means," *IEEE Journal of Selected Topics in Signal Processing*, vol. 8, no. 5, pp. 966–981, Oct 2014.

[36] W. Choi and J. G. Andrews, "The capacity gain from intercell scheduling in multi-antenna systems," *IEEE Transactions on Wireless Communications*, vol. 7, no. 2, pp. 714–725, 2008.

[37] A. M. Tulino and S. Verdú, "Random matrix theory and wireless communications," *Foundamental Trends Communication Information Theory*, vol. 1, no. 1, pp. 1–182, Jun 2004.